

1 **3D dust aerosol distribution and extinction climatology**  
2 **over North Africa simulated with the ALADIN numerical**  
3 **prediction model from 2006 to 2010**

4  
5 **Mohamed Mokhtari<sup>1,2</sup>, Pierre Tulet<sup>1,3</sup>, Claude Fischer<sup>1</sup>, Yves Bouteloup<sup>1</sup>,**  
6 **François Bouyssel<sup>1</sup>, Omar Brachemi<sup>2</sup>**

7 [1] {CNRM/GAME, UMR3589 (Météo-France, CNRS), Toulouse, France}

8 [2] {Office National de la Météorologie (ONM), Algiers, Algeria}

9 [3] {LACy, UMR8105 (Université de La Réunion, Météo-France, CNRS), Saint-Denis de La  
10 Réunion, France}

11 Correspondence to:

12 M. Mokhtari: [m\\_morad06@yahoo.fr](mailto:m_morad06@yahoo.fr), P. Tulet [pierre.tulet@univ-reunion.fr](mailto:pierre.tulet@univ-reunion.fr)

13  
14 **Abstract**

15 The seasonal cycle and optical properties of mineral dust aerosols in North Africa were  
16 simulated for the period from 2006 to 2010 using the numerical atmospheric model ALADIN  
17 coupled to the surface scheme SURFEX. The particularity of the simulations is that the major  
18 physical processes responsible for dust emission and transport, as well as radiative effects, are  
19 taken into account at short timescales and mesoscale resolution. The aim of these simulations  
20 is to quantify the dust emission and deposition, locate the major areas of dust emission and  
21 establish a climatology of aerosol optical properties in North Africa. The mean monthly  
22 Aerosol Optical Thickness (AOT) simulated by ALADIN is compared with the AOTs  
23 derived from the standard Dark Target (DT) and Deep Blue (DB) algorithms of the Aqua-  
24 MODIS (MODerate resolution Imaging Spectroradiometer) products over North Africa, and  
25 with a set of sun photometer measurements located at Banizoumbou, Cinzana, Soroa, Mbour

1 and Capo Verde. The vertical distribution of dust aerosol represented by extinction profiles is  
2 also analysed using CALIOP (Cloud-Aerosol Lidar with Orthogonal Polarization)  
3 observations.

4 The annual dust emission simulated by ALADIN over North Africa is 878 Tg.year<sup>-1</sup>. The  
5 Bodélé depression appears to be the main area of dust emission in North Africa, with an  
6 average estimate of about 21.6 Tg.year<sup>-1</sup>.

7 The simulated AOTs are in good agreement with satellite and sun photometer observations.

8 The positions of the maxima of the modelled AOTs over North Africa match the observed  
9 positions, and the ALADIN simulations satisfactorily reproduce the various dust events over  
10 the 2006-2010 period.

11 The AOT climatology proposed in this paper provides a solid database of optical properties  
12 and consolidates the existing climatology over this region derived from satellites, the  
13 AERONET network and Regional Climate Models. Moreover, the three-dimensional  
14 distribution of the simulated AOTs also provides information about the vertical structure of  
15 the dust aerosol extinction.

16

## 17 **1. Introduction**

18 Mineral dust aerosol dominates the aerosol mass over some continental regions with relatively  
19 higher concentrations accounting for about 35% of the total aerosol mass (IPCC, 2013). These  
20 terrigenous particles transported by the atmosphere significantly alter the Earth's radiative  
21 budget by absorbing and scattering incoming solar and outgoing terrestrial radiation  
22 (Haywood et al., 2001; Sokolik et al., 2001, Houghton et al., 2001). They can affect cloud  
23 properties by modifying their radiative properties and precipitation (IPCC, 2007; Twomey,  
24 1959; Albrecht, 1989; Sandu et al., 2008). They also play several roles in biogeochemical  
25 cycles (Martin, 1991; Swap et al., 1992), atmospheric chemistry (Wang et al., 2002; Martin et  
26 al., 2003), visibility and human health. Because of the important role that dust might play in

1 future climate change and its potential high impact on the Earth's ecosystems and natural and  
2 human environments, it is important to know where the major dust sources are, how dust  
3 concentration varies in space and time and what controls this variability. North Africa is the  
4 world's main source of dust aerosol, with a relative contribution of about 50% of the total  
5 worldwide production (Zender et al., 2003a). This region is well suited for studying the  
6 impact of aerosols on the radiation budget and climate. Therefore, an accurate database of  
7 aerosol content in this region is crucial to identify and quantify this impact, particularly in  
8 Regional Climate Models (RCMs). Changes to this database in numerical models have a  
9 sensitive impact on model performance. For example, various studies (Tompkins et al., 2005;  
10 Rodwell, 2005) have shown the positive impact of the switch from the Tanré et al. (1984)  
11 climatology to the Tegen et al. (1997) climatology for various aspects of the ECMWF model  
12 (Morcrette et al., 2009). Tompkins et al., (2005) have performed a couple of 5-day forecasts  
13 of the African Easterly Jet (AEJ) with the old and new climatology and the results are  
14 compared with high resolution dropsonde data from the JET2000 campaign. The results of  
15 these simulations show that the new aerosol climatology significantly improves some aspects  
16 of the AEJ structure and strength. In the same study, 4 months of 5-day forecasts was realized  
17 and compared using the contrasting aerosol distributions. The results show a clear  
18 improvement with the new climatology, with the jet strengthened, elongated to the east, and  
19 less zonal, in agreement with the analyses. The new climatology suppresses deep convection  
20 by stabilizing the atmosphere, preventing the ITCZ from progressively migrating north during  
21 the forecast. A strong reduction of mean equivalent potential temperature at the lowest model  
22 level is noted, with the southerly displacement of the ITCZ. More recently, Kocha et al.  
23 (2012) have shown the impact of dust storms on the cold extra-tropical outbreak and on the  
24 African Easterly Jet.

1 Today, several datasets for aerosol parameters in North Africa are available. The Aerosol  
2 Robotic Network (AERONET; <http://aeronet.gsfc.nasa.gov/>, Holben et al., 1998), with its  
3 specifically designed geographical coverage, provides a robust database of aerosol optical  
4 thickness, while the data itself describes local characteristics at station positions. Satellite  
5 products allow the spatial and temporal variability of atmospheric dust aerosol concentrations  
6 to be studied (Brooks and Legrand, 2000; Prospero et al., 2002; Washington et al., 2003).  
7 These products provide a two dimensional (2D) horizontal representation of dust plumes and  
8 offer maximum spatial coverage. Numerous studies have been conducted to reproduce the  
9 dust aerosol contents in North Africa based on this type of data. For example, Engelstaedter et  
10 al. (2006) used the TOMS (Total Ozone Mapping Spectrometer) AAI (Absorbing Aerosol  
11 Index) product from 1980 to 1992 to identify Saharan dust source regions and create a  
12 qualitative description of the annual dust cycle.

13 In the infrared spectrum, the Meteosat IDDI (Infrared Difference Dust Index) products are  
14 also available. Brooks and Legrand (2000) used IDDI to localize the dust emission regions  
15 over northern Africa for the period 1984-1993. In addition, very high resolution AOT data is  
16 now available from satellites such as MODIS, MISR (Multi-angle Imaging  
17 SpectroRadiometer) and SEAWIFS (Sea-viewing Wide Field-of-view Sensor) and inversion  
18 codes such as Deep Blue ([http://gdata1.sci.gsfc.nasa.gov/daac-](http://gdata1.sci.gsfc.nasa.gov/daac-bin/G3/gui.cgi?instance_id=aerosol_daily)  
19 [bin/G3/gui.cgi?instance\\_id=aerosol\\_daily](http://gdata1.sci.gsfc.nasa.gov/daac-bin/G3/gui.cgi?instance_id=aerosol_daily)). Indeed, a recent comparative study (Bréon et al.,  
20 2011) between AOTs derived from POLDER (Polarization and Directionality of Earth's  
21 Reflectances), MODIS, MERIS (Medium Resolution Imaging Spectrometer), SEVIRI  
22 (Spinning Enhanced Visible and Infrared Imager) and CALIOP (Cloud-Aerosol Lidar with  
23 Orthogonal Polarization) shows that MODIS has the most reliable estimate of total AOT over  
24 ocean and land. However, this data encompasses the collective contributions of maritime,  
25 continental and desert dust aerosols. Furthermore, the quality of satellite dust products is

1 affected by a number of uncertainties related to the spatial/temporal resolution, atmospheric  
2 conditions and range of wavelengths used by each satellite. These error sources are  
3 thoroughly discussed in Schepanski et al. (2012). For example, Kocha et al. (2013) have  
4 indicated that the specific transit time of MODIS over West Africa generates a bias in the  
5 AOT dust retrieval due to the diurnal cycle of atmospheric processes such as convection and  
6 the early morning low-level jet.

7 Numerical modelling provides a three-dimensional view of the atmosphere and can be used to  
8 evaluate the individual role of each parameter involved in the optical thickness. The Tegen et  
9 al. (1997) climatology gives an average distribution valid for one year (1990), obtained from a  
10 combination of global distributions of aerosol data from different transport models for soil  
11 dust (Tegen and Fung, 1995), sea salt (Tegen et al., 1997), sulfates (Chin et al., 1996) and  
12 carbonaceous aerosols (Liousse et al., 1996). However, due to its low spatial resolution ( $5^\circ \times$   
13  $4^\circ$ ), the content of dust aerosol over North Africa is not well represented. Recently, Kinne et  
14 al. (2013) proposed a new monthly global climatology, MAC-v1 (Max-Planck-Institute  
15 Aerosol Climatology version 1) with a  $1^\circ \times 1^\circ$  resolution. This climatology addresses 3 aerosol  
16 properties, namely the AOT, which provides information on the amount of aerosol, the SSA  
17 (Single scattering albedo), which provides information on absorption and the  $A_p$  (Angström  
18 parameter), which provides information on size distribution.

19 Based on both satellite-derived monthly AOTs and a regional/chemistry model, Nabat et al.  
20 (2013) proposed a three-dimensional (3-D) monthly climatology of aerosol distribution over  
21 the Mediterranean Sea for the 1979-2009 period and at 50 km of resolution.

22 Initiatives have already been taken to use operational Numerical Weather Prediction (NWP)  
23 and regional models at high resolution and short timescales. These efforts include the WMO  
24 Sand and Dust Storm Warning Advisory and Assessment (SDS-WAS, <http://sds->

1 was.aemet.es) program, whose mission is to achieve comprehensive, coordinated and  
2 sustained observations and modeling of sand and dust storms in order to improve the  
3 monitoring of such storms, increase understanding of the dust processes and enhance dust  
4 prediction capabilities. SDS-WAS is established as a federation of partners organized around  
5 regional nodes (Northern Africa-Middle East-Europe Node and Asian Node). About 16 dust  
6 prediction models have been used in SDS-WAS as BSC-DREAM8b, MACC-ECMWF,  
7 INCA-LMDZT, CHIMERE, SKIRON, ETA, NGAC, NAAPS....

8 In this study, data and results from simulations using the ALADIN model over North Africa  
9 from 2006 to 2010 are presented. This model takes into account the different physical  
10 processes responsible for the emission, transport and deposition of dust. The aim of these  
11 simulations is to quantify the annual and seasonal emissions, locate the main emission dust  
12 sources and establish a climatology of dust aerosol optical properties in North Africa. The  
13 mean monthly Aerosol Optical Thickness simulated by ALADIN is evaluated with the AOTs  
14 derived from the standard Dark Target and Deep Blue algorithms of the Aqua-MODIS  
15 products over North Africa and a set of sun photometer measurements located at  
16 Banizoumbou, Cinzana, DMN\_Maine\_Soroa (hereafter Soroa), Mbour and Capo Verde. In  
17 order to validate the ALADIN vertical distribution of aerosols, we use the mean extinction  
18 profiles derived from CALIOP.

19 The paper is organised as follows. A brief description of the ALADIN model and the  
20 methodology for analysing the data is given in Section 2. The numerical results of dust  
21 emission, dry and wet deposition, AOT, and extinction coefficients are discussed in Section 3.  
22 The comparison of the modelled data with Aqua-MODIS products, AERONET datasets,  
23 surface concentration observation and CALIOP observation is presented in Section 4. Section  
24 5 is devoted to the concluding discussion.

## 1    **2.    Tools and methods**

### 2    **2.1    Model description and dust transport**

3    The spectral hydrostatic atmospheric numerical prediction model ALADIN is used in this  
4    study. ALADIN is a primitive equations model using a two-time-level semi-Lagrangian semi-  
5    implicit time integration scheme and a digital filter initialisation (Bubnová et al., 1995;  
6    Radnóti, 1995). The atmospheric prognostic variables of the model comprise the wind  
7    horizontal components, temperature, and specific humidity fields of water vapour and the  
8    four types of hydrometeors (cloud droplets, ice crystals, rain and snow), as well as the  
9    turbulent kinetic energy. The influence of subgrid physical processes (radiation,  
10    microphysics, turbulence, convection, gravity waves, surface processes) on the evolution of  
11    the model's prognostic variables is represented with physical parameterizations. The radiative  
12    transfer in the atmosphere (gaseous, clouds, ozone, and aerosols) and with the surface is  
13    described using the RRTM scheme (Rapid Radiative Transfer Model) for longwave radiation  
14    (Mlawer et al., 1997) and the six-band Fouquart-Morcrette scheme for shortwave radiation  
15    (Fouquart et al., 1980, Morcrette, 1991). Several phenomena linked to the subgrid orography,  
16    such as gravity waves, their reflection and trapping, as well as upstream blocking, are taken  
17    into account (Catry et al., 2008). The transport in the atmospheric boundary layer is  
18    represented with a diffusion scheme based on prognostic turbulent kinetic energy (Cuxart et  
19    al., 2000) using the Bougeault and Lacarrère (1989) mixing length, and on a mass flux  
20    shallow convection scheme using a CAPE closure (Bechtold et al., 2001). Deep convection is  
21    represented with a mass flux scheme based on a moisture convergence closure (Bougeault,  
22    1985). A statistical cloud scheme (Smith, 1990; Bouteloup et al., 2005) is used for the  
23    representation of stratiform clouds. Microphysical processes such as auto-conversion,  
24    collection, evaporation, sublimation, melting and sedimentation are represented following the

1 parametrization of Lopez (2002). Surface processes are calculated using the externalized  
2 surface scheme SURFEX (SURFace EXternalisée) (Masson et al., 2013) which includes the  
3 Interaction Soil Biosphere Atmosphere (ISBA) scheme (Noilhan and Planton, 1989). This  
4 model configuration is very close to the operational configurations used at Météo-France-- in  
5 ALADIN Overseas applications, for instance--and in about 16 National Weather Services  
6 members of the ALADIN consortium.

7 Dust transport and optical properties are calculated using the three-moment Organic Inorganic  
8 Log-normal Aerosol Model (ORILAM) (Tulet et al., 2005). ORILAM predicts the evolution  
9 of the aerosol composition, along with the number, mean radius, and standard deviation of the  
10 aerosol distribution (Binkowski and Roselle, 2003). The method of calculation of aerosol  
11 optical properties is described in Grini et al., (2006). The refraction indexes used in our work  
12 have been calculated following a table of interpolation proposed by Grini et al., (2006). The  
13 dust optical properties are calculated from these new indexes in function of lognormal  
14 parameter upon the AMMA size distribution (Tulet et al., 2008). ORILAM has been  
15 evaluated in several papers for the West Africa region. Crumeyrolle et al., (2008 and 2011)  
16 presented a thorough description of the size distribution for the AMMA campaign. Mallet et  
17 al., (2009) studied the evolution of the asymmetry factor ( $g$ ) and the single scattering albedo  
18 (SSA) for the dust storm event of March 2006 and studied the radiative balance over West  
19 Africa. Such specific studies however only can be carried out for particular situations. Dry  
20 deposition is calculated according to Seinfeld and Pandis (1997) using the resistance concept  
21 from Wesely (1989). Sedimentation of aerosols is driven by the gravitational velocity (Tulet  
22 et al., 2005).



1 The wet removal of dust aerosols is calculated using the SCAVenging submodel (Tost et al.,  
2 2006; Tulet et al., 2010). The dry deposition and sedimentation are driven by the Brownian  
3 diffusivity (Tulet et al., 2005).

## 4 **2.2 Dust emission model**

5 The dust fluxes are calculated using the Dust Entrainment And Deposition (DEAD) model  
6 (Zender et al., 2003a). The physical parameterizations in the DEAD scheme are based on the  
7 Marticorena and Bergametti (1995) scheme, in which dust is calculated as a function of  
8 saltation and sandblasting. The dust mobilization starts when the wind friction velocity over  
9 an erodible surface exceeds a threshold value (Bagnold, 1941; Chepil, 1951). This threshold  
10 friction velocity is controlled primarily by surface and soil conditions (surface roughness, soil  
11 size distribution ...).

12 DEAD was implemented in the ISBA scheme embedded in SURFEX (Grini et al., 2006).  
13 Recently this emission parameterization has been improved by Mokhtari et al. (2012), in  
14 order to better account for the soil aggregate distribution.

15 The erodible soil fraction is related to bare and rock soil. These surface types are derived from  
16 the global dataset of land surface ECOCLIMAP at 1 km resolution which combines the global  
17 land cover maps at 1/120° resolution and satellite information (Masson et al., 2003). Two  
18 hundred and fifteen ecosystems were obtained by combining existing land cover and climate  
19 maps, in addition to using Advanced Very High Resolution Radiometer (AVHRR) satellite  
20 data. The ECOCLIMAP database is designed in compliance with the SURFEX “tile”  
21 approach: each grid box is composed of four adjacent surfaces for nature (ISBA vegetation  
22 classes), urban areas (TEB model), sea or ocean and lake. The mass fractions of clay, sand  
23 and silt are provided from the global 10 km FAO soil datasets. Soil texture is classified  
24 following the USDA (1999) (United States Department of Agriculture) textural classification

1 with 12 basic textural definitions. Soil aggregate size distributions are defined for each  
2 texture.

3 For the size distribution of the emitted dust, we adopted Crumeyrolle et al.'s proposal (2011)  
4 based on the measurements taken during the AMMA Special Observation Period (SOP) of  
5 June 2006. The different parameters related to this distribution are shown in table I.

### 6 **2.3 2006-2010 simulations**

7 The ALADIN model is coupled to the ARPEGE global model, which provides the initial and  
8 boundary conditions every 3 hours. To simulate the 2006–2010 period, successive forecasts of  
9 two consecutive days (48 h) are performed. The final term of each simulation is used as the  
10 initial condition for the dust concentration of the next simulation. The model simulation has a  
11 spin-up period and in order to start our study with a realistic initial state for dust  
12 concentrations, the start date of the numerical simulations is 25 December 2005. However, for  
13 the evaluations described in this article, only data from 1 January 2006 through 31 December  
14 2010 are considered. The numerical integrations are performed over a fairly large domain  
15 (4°S-40°N, 40°W-50°E) including all dust emission sources in the Sahara and those of the  
16 Western part of the Arabian Desert. This choice minimizes the prediction errors in dust  
17 concentrations due to lateral coupling, as no dust modelling is included in the coupling global  
18 model. Here, care was taken to ensure that no dust emission zone was present outside and  
19 near the limited area domain. The post-processing domain was intentionally decreased in  
20 order to facilitate the exploitation of results; it extends from 2°N to 38°N and from 39°W to  
21 45°E. The horizontal resolution is 20 km x 20 km with 60 hybrid vertical levels; from the  
22 surface to 67 km. The time step is 600 s. In this paper, we restrict the analysis to the  
23 extinction coefficient and its vertical integration (AOT) for comparison with the observations  
24 available for the 2006-2010 period.

## 1   **2.4    Dataset**

2

### 3   **2.4.1   Ground-based measurement**

4   In this study we use the AERONET AOT product (level 2) and the PM10 measured dust mass  
5   concentration (Particulate Matter concentration, particles with diameter of 10  $\mu\text{m}$  or less) in  
6   order to evaluate the model-simulated AOT and the surface dust concentration, respectively,  
7   from 2006 to 2010.

8   AERONET (<http://aeronet.gsfc.nasa.gov/>) is a federation of ground-based remote sensing  
9   instruments measuring aerosol and its characteristics (Holben et al., 1998). The AERONET  
10   sunphotometers directly measure aerosol optical thickness at seven wavelengths  
11   (approximately 0.340, 0.380, 0.440, 0.500, 0.675, 0.870, and 1.02  $\mu\text{m}$ ) with an estimated  
12   uncertainty of 0.01 – 0.02 (Holben et al., 2001). In the model, the AOT is simulated at 0.55  
13    $\mu\text{m}$ , and it is therefore compared to the AOT measured at the nearest wavelength, 0.440  $\mu\text{m}$  or  
14   0.675  $\mu\text{m}$ . Following Schmechtig et al., (2011) the AOT measured over Banizoumbou,  
15   Cinzana and Mbour, at wavelength 0.44  $\mu\text{m}$  and 0.675  $\mu\text{m}$ , are significantly correlated ( $r^2$   
16   =0.99) with slopes ranging from 1.04 in Cinzana to 1.06 in MBour. Thus, in our study, we  
17   used the AOT measured at 0.44  $\mu\text{m}$  over the five AERONET sites located in West Africa at:  
18   Banizoumbou (Niger), Cinzana (Mali), DMN\_Maine\_Soroa (Niger), Mbour (Senegal) and  
19   Capo Verde (Fig. 1). We note that the AOT measurements only are possible during the day  
20   since they are based on measuring the solar radiation attenuation. This characteristic may be  
21   affecting the results of the intercomparison if a dust storm event occurred at night-time.

22   The three stations composing the “Sahelian Dust Transect” (SDT) (Marticorena et al., 2010)  
23   located in the Sahelian region at Banizoumbou, Cinzana and MBour are used to validate the  
24   surface dust concentration simulated by ALADIN. The SDT provides a continuous  
25   monitoring of the atmospheric concentrations PM10 with a 5 minute time step, using a  
26   Tapered Element Oscillating Microbalance (TEOM 1400A from Thermo Scientific) equipped

1 with a PM10 inlet. PM10 measurements refer to particulate matter which passes through a  
2 size-selective inlet with a 50% efficiency cutoff at 10  $\mu\text{m}$  aerodynamic diameter (Marticorena  
3 et al., 2010). In terms of sensitivity, the detection limit of the instrument is about  $0.06 \mu\text{g}\cdot\text{m}^{-3}$   
4 for a one hour sampling time.

5

#### 6 **2.4.2 Satellite data**

7 The Aqua-MODIS product (Tanré et al., 1997; Levy et al., 2007) was used to evaluate the  
8 AOTs simulated by ALADIN. This instrument is a multi-spectral radiometer, designed to  
9 retrieve aerosol microphysical and optical properties over ocean and land. Two products of  
10 Aqua-MODIS are considered in this study: the MODIS Dark Target (DT) and the MODIS  
11 Deep Blue (DB) algorithms (Hsu et al., 2004). The MODIS DT algorithm over land is not  
12 designed to retrieve aerosol over bright surfaces, such as the Saharan deserts due to the large  
13 values of surface reflectivity (Remer et al., 2005; Shi et al., 2013). This problem leads to large  
14 spatial gaps in the aerosol optical thickness recorded in desert regions, although these regions  
15 are affected by some of the largest aerosol loadings worldwide. However, the DB algorithm  
16 takes advantage of this surface phenomenology by performing aerosol retrievals in the visible  
17 blue spectrum (such as the  $0.47 \mu\text{m}$  spectral channel in MODIS) and by utilizing the selected  
18 aerosol model in the inversion to generate the AOT (Hsu et al., 2004, 2006; Shi et al., 2013).  
19 Thus, a combination between these two products is made to complete the AOT database for  
20 the whole of North Africa (ocean and land).

21 Over bright arid region, only DB data are available, offering no alternative choice.  
22 Conversely, in the areas with dense vegetation and ocean, only DT data are available and are  
23 therefore used in our study, in these regions. In addition, we have transition areas with low  
24 vegetation such as the Sahel ( $10^{\circ}\text{N}$ - $15^{\circ}\text{N}$ ). For these areas, both the DB and DT products are  
25 available. The DT product for the semi-arid regions tends however to be biased and

1 underestimated (Levy et al., 2010). For example, the difference between DB and DT  
2 estimated for the transition regions can exceed 0.3. For this reason we chose the DB product  
3 for the transition regions. Recently, Levy et al., (2013) proposed another solution for the  
4 transition regions, namely to merge the two products and create a combined AOD product.  
5 Levy et al., (2013) used the Normalized Difference Vegetation Index (NDVI) to identify these  
6 regions. Unfortunately, this solution has not yet been validated.

7 The CALIOP Level 2 Layer 5 km product was used to evaluate the mean particle vertical  
8 distributions simulated by ALADIN over North Africa. The CALIOP instrument (Winker et  
9 al., 2007) was launched in 2006 on the Cloud–Aerosol Lidar and Pathfinder Satellite  
10 Observations (CALIPSO) spacecraft, and has now provided over 8 years of nearly continuous  
11 global measurements of aerosols and clouds with high vertical and spatial resolution at two-  
12 wavelength (532 nm and 1064 nm) (Rogers et al., 2014). As part of the “A-train”  
13 multisatellite constellation, CALIPSO follows a 705 km sun-synchronous polar orbit, with an  
14 equator-crossing time of about 1:30 P.M., local solar time (Stephens et al., 2002). The orbit  
15 repeats the same ground track every 16 days. The vertical distribution of aerosols, provided  
16 by lidar, is important for radiative forcing (e.g., Satheesh, 2002), air quality studies (e.g., Al-  
17 Saadi et al., 2005; Engel-Cox et al., 2006), and model validation (Dirksen et al., 2009; Koffi  
18 et al., 2012). The CALIOP instrument and its initial performance assessment are described in  
19 Winker et al. (2007) and Hunt et al. (2009).

## 20 **3. Results**

### 21 **3.1 Dust emissions**

#### 22 **3.1.1 Annual dust emissions and Interannual variability**

23 Figure 2 shows the annual mean dust emissions over the Sahara averaged from 2006 to 2010  
24 simulated by ALADIN coupled on-line with the ORILAM aerosol scheme and the DEAD

1 version of Mokhtari et al., (2012). The major dust sources are located over the Bodélé  
2 Depression with an annual mean dust flux around  $2 \text{ kg.m}^{-2}.\text{year}^{-1}$ , the centre of Niger ( $400-$   
3  $600 \text{ g.m}^{-2}.\text{year}^{-1}$ ), the oriental and occidental great Erg in Algeria ( $200-400 \text{ g.m}^{-2}.\text{year}^{-1}$ ), the  
4 Western Sahara coast, the centre of Mauritania and Mali ( $200-400 \text{ g.m}^{-2}.\text{year}^{-1}$ ), the  
5 southeastern region of Libya and Sudan ( $100-200 \text{ g.m}^{-2}.\text{year}^{-1}$ ), and along the border between  
6 Egypt and Libya ( $100-200 \text{ g.m}^{-2}.\text{year}^{-1}$ ).

7 The averaged annual dust emission over the whole Sahara and for the 5 years of simulation is  
8  $878 \text{ Tg}.\text{year}^{-1}$ . Annual dust emissions vary from  $843 \text{ Tg}$  in 2010 to  $924 \text{ Tg}$  in 2008. Table 2  
9 compares the annual mean dust flux obtained in this work with other recent global and  
10 regional dust model studies. Important differences in the annual mean dust flux can be  
11 observed. The largest value of the annual mean dust flux is simulated by Ginoux et al. (2004)  
12 and is equal to  $1430 \text{ Tg}.\text{year}^{-1}$ , which is twice as large as the value simulated by Marticorena  
13 and Bergametti (1996) ( $665-586 \text{ Tg}.\text{year}^{-1}$ ). Our estimation lies between those obtained by  
14 Ginoux et al. (2004) and by Marticorena and Bergametti (1996), and is in good agreement  
15 with the value obtained by d'Almeida (1986), Callot et al. (2000), Laurent et al. (2008) and  
16 Zender et al. (2003).

17 Dust emissions depend on both surface features and soil types, but they also depend on the  
18 meteorological conditions (wind and precipitation). These elements are defined differently  
19 from one model to another. Global models have a relatively low resolution, and thus  
20 misrepresent the surface characteristics (roughness) and the soil types (% of clay and % of  
21 sand). As a consequence, these models tend to overestimate the spread of dust emission areas.  
22 For example, at  $1^\circ \times 1^\circ$  resolution (medium resolution of global models), an entire area can  
23 become a dust emission source when in reality it is not. Eventually, dust emission is  
24 overestimated as well. Regional models, due to their higher resolution, provide more details

1 on the emission source areas compared with global models, which then in turn enables to  
2 diminish this positive bias.

3 It is also interesting to mention that the three values of dust emission estimated by Zender et  
4 al., (2003), Laurent et al., (2008), Marticorena et al., (1995) and the one of our study are all  
5 based on the same dust mobilization scheme of Marticorena et al. (1995). Therefore, a  
6 correlation between the estimates of these four studies can be expected. Over the Bodélé  
7 depression (10800 km<sup>2</sup>), the annual mean dust emission is estimated at 21.4 Tg.year<sup>-1</sup>.  
8 Although this region represents only 0.13% of the Sahara, its contribution is around 2.4% of  
9 the annual mean dust flux of the whole Sahara. This finding is in good agreement with  
10 previous studies of this region (Zender et al., 2003a). Based on field observations, Todd et al.  
11 (2007) suggest that the emission of aerosols minerals from the Bodélé Depression is  $1.18 \pm$   
12  $0.45$  Tg.day<sup>-1</sup> during a substantial dust event.

13 Figure 3 presents the monthly emissions in Tg from January 2006 to December 2010. This  
14 figure shows that the largest monthly emissions are generally obtained in spring. During the  
15 5-year simulated period, a maximum (120 Tg per month) is simulated in March 2010 and the  
16 minimum (35 Tg per month) is obtained in December 2009.

### 17 **3.1.2 Seasonality of the dust emissions**

18 Figure 4 shows the seasonal mean dust emissions from 2006 to 2010. The seasonal cycle is  
19 characterized by a maximum of dust emission in spring. All possible dust sources are  
20 activated during this season. The minimum dust emissions are simulated in autumn, except  
21 over the Bodélé region. In summer, dust emission remains strong in the Western Sahara,  
22 while it decreases in the Eastern Sahara. In winter, dust emission sources are mainly located  
23 in the Bodélé depression and the centre of Niger. These regions are indeed frequently exposed  
24 to the Harmattan wind during the dry monsoon season, which is a favourable configuration

1 for dust emission. In spring and autumn, dust emission remains significant over the Bodélé  
2 Depression, but the dust emission activity decreases in summer. This seasonality is in  
3 agreement with the six-year simulation by Laurent et al. (2008) (1996-2001) and the  
4 simulation by Schmechtig et al. (2011) for 2006.

5 Figure 5 presents the seasonal mean and interseasonal dust emissions over the Sahara during  
6 the 5-year period. Our simulations estimate the seasonal mean dust emissions in spring at  
7 around 296 Tg. In summer, the seasonal emissions remain significant, at about 233 Tg. In  
8 winter and autumn, our estimations are 196 Tg and 150 Tg, respectively. This seasonality  
9 reproduces the general pattern of the seasonality simulated by Tanaka and Chiba (2005) for  
10 the period 1979–2003 over North Africa with the global CTM model (MASINGAR) at a  
11 resolution of  $1.8 \times 1.8^\circ$ . In contrast, in terms of intensity, the dust emission flux simulated by  
12 MASINGAR in spring accounts for almost half of the total emissions in North Africa (500  
13 Tg). These estimates are higher than those simulated by ALADIN.

14 In summer, the dust emission flux simulated by MASINGAR is much underestimated  
15 compared with the flux estimated by ALADIN. Indeed, the summer season is characterized  
16 by significant dust uprising over the Sahel in connection with large convective systems. These  
17 systems generate strong gust winds at the leading edge of their cold pools which can lead to  
18 “walls of dust” known as "haboob", a sometimes fast moving and extremely hazardous  
19 phenomenon (Knippertz et al. 2012). However, even regional models at resolution of about 10  
20 km do not adequately represent these processes, neither in climatological terms nor for  
21 weather forecasting (Knippertz et al. 2012).

## 22 **3.2 Dry deposition**

23 The annual dry deposition of mineral dust over North Africa is another estimated product of  
24 the ALADIN integrations. Generally, regions of dry deposition are located near dust emission



1 regions, as most of the emitted dust mass is of the coarse type, which settles quickly. Thus, in  
2 the Bodélé Depression, the dust mass subject to dry deposition is at its maximum (400-800  
3  $\text{g.m}^{-2}.\text{year}^{-1}$ ), and corresponds to around half the annual dust emission. The Ergs located in the  
4 centre of Mauritania, Mali, Niger, and the great Eastern and Western Erg in Algeria, Western  
5 Sudan, South-West of Egypt and Libya come in second, with dry deposition values between  
6 100-300  $\text{g.m}^{-2}.\text{year}^{-1}$ . The mountainous and rocky deserts have a dry deposition ranging from  
7 40-100  $\text{g.m}^{-2}.\text{year}^{-1}$ .

8 The seasonal mean dry deposition flux is shown in Fig. 6. The southern boundary of the dry  
9 deposition area is modulated by the position of the Inter Tropical Convergence Zone (ITCZ).  
10 In winter, the maximum of the seasonal dust deposition flux is located in the Bodélé  
11 Depression, with a value reaching 200  $\text{g.m}^{-2}$ . This maximum is a consequence of low level  
12 dust transport during this period. The geographical extension of the dry deposition areas is  
13 very large, especially towards the south and the west of the Sahara, which are the main areas  
14 of dust transport (Swap et al., 1992; Kaufman et al., 2005). The area of dust deposition of  
15 more than 10  $\text{g.m}^{-2}$  extends southward to about 5°N and covers the subtropical Atlantic. In  
16 spring, the mean seasonal dust deposition flux is high over the great Eastern and Western Erg  
17 in Algeria (150  $\text{g.m}^{-2}$ ), but decreases over the Bodélé Depression and Niger. In this season,  
18 the southern limit of the extension of the mean seasonal dry deposition area ( $>10 \text{ g.m}^{-2}$ ) is at  
19 10 °N. In summer, this limit is located around 15°N, in connection with the establishment of  
20 the West African monsoon and the migration of the ITCZ towards the north. This season is  
21 characterized by high precipitation over West Africa, which is very efficient at suppressing  
22 dust emission and generates significant washout. In autumn, in conjunction with the decrease  
23 of the dust emission activity over the Sahara, the mean seasonal dust deposition decreases,  
24 except in the Bodélé Depression.

### 1 3.3 Wet deposition

2 In this section, we show that the use of a three-dimensional NWP model such as ALADIN  
3 significantly improves the climatology of wet deposition of dust aerosols. Indeed, the model  
4 provides a representation of large-scale and mesoscale precipitating processes, with a spatial  
5 and temporal resolution and operational-like calibration of the schemes, which provides  
6 insight into regional and seasonal aspects of wet deposition.

7 Figure 7 presents the mean seasonal wet deposition flux simulated by ALADIN over North  
8 Africa, averaged for the 2006-2010 period. The localization of wet deposition areas depends  
9 mainly on the distribution of large-scale and convective precipitations and the direction of  
10 dust plume transport. In winter, during the dry West African monsoon season, the mean wet  
11 deposition fluxes simulated by ALADIN do not exceed  $10 \text{ g.m}^{-2}$  in the Sahara and Sahelian  
12 regions. In contrast, wet deposition is very active ( $20$  to  $60 \text{ g.m}^{-2}$ ) in the band from  $0^\circ$  to  $10^\circ\text{N}$   
13 over the gulf of Guinea and the Atlantic Ocean. In spring, the highest mean wet deposition  
14 flux is observed over the south of Niger, with values exceeding  $40 \text{ g.m}^{-2}$ . Summer is the  
15 season of the wet African monsoon, characterized by large convective systems over the  
16 Sahelian regions. These systems play a key role in the wet deposition of mineral dust  
17 aerosols. Since these convective systems produce aerosols in the gust front, the associated  
18 aerosols are to a large extent washed out by precipitation (Flamant et al., 2007; Tulet et al.,  
19 2010). As a consequence, in our simulation, ALADIN simulates the maximum wet deposition  
20 in the band from  $15^\circ \text{N}$  to  $20^\circ \text{N}$ . This band corresponds to western Chad, central Niger, Mali  
21 and Mauritania, with average values of  $60$ - $140 \text{ g.m}^{-2}$ . Autumn is characterized by the turning  
22 of the African monsoon and the southward displacement of the ITCZ, in conjunction with a  
23 decrease in precipitation and wet deposition over the Sahelian region. We note that, beyond  
24  $10^\circ\text{N}$ , wet deposition processes are more efficient than dry deposition.

1 The inter-comparison of dust wet deposition simulated by ALADIN for the year 2006 with  
2 models used in the AEROCOM and SDS-WAS programs (BSC-DREAM8b, GOCART-  
3 v4Ed.A2.CTRL, GISS-modelE.A2.CTRL and TM5-V3.A2.CTRL, [http://aerocom.met.no/cgi-  
4 bin/aerocom/surfobs\\_annualrs.pl](http://aerocom.met.no/cgi-bin/aerocom/surfobs_annualrs.pl)) for the same period is given by the Table 3. The results  
5 show that the mean wet deposition estimated by ALADIN is much higher than those  
6 estimated by AEROCOM Model's. As discussed for the seasonal wet deposition, the major part  
7 of the wet deposition takes place during the wet season of the African Monsoon.

8 In terms of spatial distribution, the ALADIN model performs better for the estimation of the  
9 dust wet deposition associated with convective systems in the Sahelian regions. For example,  
10 the estimates of the BSC-DREAM8b model do not exceed  $0.2 \text{ g.m}^{-2}.\text{year}^{-1}$  for the Sahel and  
11 the West African region. Those simulated by TM5-V3.A2.CTRL are less than  $5 \text{ g.m}^{-2}.\text{year}^{-1}$   
12 and those obtained by GOCART-v4Ed.A2.CTRL and GISS-modelE.A2.CTRL varied in the  
13 range  $20\text{-}50 \text{ g.m}^{-2}.\text{year}^{-1}$ . The fact that some part of the total precipitation of ALADIN is  
14 resolved can explain that the wet deposition processes in ALADIN are found to be more  
15 efficient than in some global models.

16

### 17 **3.4 Monthly variation of Aerosol Optical Thickness**

18 Figure 8 shows the monthly aerosol optical thickness averaged from 2006 through 2010 over  
19 North Africa. The monthly variation is characterized by two maxima of AOT exceeding 1.2.  
20 The first maximum is simulated in March and is located over the Sahelian region in West  
21 Africa. This maximum is correlated with the high dust emissions observed in the Bodélé  
22 depression and the centre of Niger. The second maximum is simulated in July and is located  
23 over Mauritania and Mali. This maximum is related to the appearance of the heat low in these  
24 regions and to the northward movement of the ITCZ in July. Low values of AOTs are  
25 registered in autumn. This season is characterized by low dust emission activity, and the

1 simulated AOTs do not exceed 0.8. Over the southern part of the Mediterranean Sea (Libyan  
2 and Egyptian coast), the AOTs due to dust are significant in spring and summer, with a  
3 monthly peak of 0.5 in July. Note that, using both satellites and a regional chemistry model,  
4 Nabat et al. (2013) found, for the 1979-2009 period, a value of 0.3 of AOT for these regions  
5 with a peak in June.

6 In terms of extension, the spatial distribution of AOTs follows the preferred dust transport  
7 direction in North Africa. The large values of AOT (0.6 to 1.2) are located in the south of the  
8 domain, between 5°N and 20°N of latitude, from December to March. In contrast, beyond  
9 20°N of latitude, the AOTs do not exceed 0.4 for this period. From April to August, the  
10 regions with large AOTs (0.6 to 1.2) follow the northward displacement of the ITCZ.  
11 Accordingly, in the ALADIN simulation, these regions extend fairly far north (> 10°N),  
12 covering major parts of the Western Sahara and the Sahelian regions. In addition, a band of  
13 high AOT (0.4 to 0.8), associated with the westward transport of dust aerosols towards the  
14 Atlantic Ocean, is simulated between 10°N and 25°N. From September to November the dust  
15 aerosol activity decreases and the regions of high AOT (0.6 to 0.8) are localised to only part  
16 of the Sahelian region and the Bodélé Depression. The spatial distribution of AOT simulated  
17 by ALADIN is well correlated with the monthly average of the AAI (Absorbing Aerosol  
18 Index) derived from TOMS data, found by Engelstaedter et al. (2006) for the 1980-1992  
19 period, especially for May, June, July and August. However, noticeable differences are  
20 observed between AOT and AAI fields in winter, especially for the month of March, which  
21 corresponds to a minimum of AAI and a maximum of AOT.

### 22 **3.5 Monthly variation of extinction coefficients**

23 The vertical distribution of aerosols in the troposphere is important for assessing their effects  
24 on climate, and is a key parameter in the objective evaluation of radiative forcing (Li et al.,  
25 2005; Kinne et al., 2006; Zhu et al., 2007). Meloni et al. (2005) found that the intensity of

1 shortwave radiative forcing at the top of the atmosphere is strongly dependent on the vertical  
2 distribution of aerosols. In this paper, we show the monthly variation of the vertical  
3 distribution of mineral dust from the surface to 10 km of altitude. In order to emphasize this  
4 distribution for low altitudes, we chose the logarithmic scale for the vertical coordinate. The  
5 vertical distribution is represented by the vertical cross section of the extinction coefficients  
6 averaged longitudinally from 30°W to 40°E and from 2006 to 2010 (Fig. 9). The maximum of  
7 the extinction coefficient is simulated in January and February and reaches  $0.36 \text{ km}^{-1}$ . This  
8 maximum is located in the lowest layer ( $< 100 \text{ m}$ ) between 12°N and 17°N with a vertical  
9 inclination toward the south. The southward inclination observed above 1.5 km of altitude is  
10 due to the location of dust aerosols in the Saharan Atmospheric Layer (SAL) and their  
11 transport by the Harmattan wind above the monsoon flux. This vertical structure is mainly  
12 observed in winter during the dry West African monsoon. In this season, a strong gradient of  
13 extinction coefficients can be observed at the surface around the ITCZ (5°N-15°N), with  
14 values varying from  $0.09 \text{ km}^{-1}$  to  $0.36 \text{ km}^{-1}$ . In altitude, over the monsoon flux (1.5 km to 3  
15 km), the extinction coefficients are relatively large ( $0.09 \text{ km}^{-1}$ ). The annual minimum of the  
16 maximum values of extinction are simulated in September and October and do not exceed  
17  $0.12 \text{ km}^{-1}$ , with a vertical extension limited to below 4 km. In summer, the onset of the West  
18 African monsoon and the northward movement of the ITCZ confine the transport of dust to  
19 the south. Instead, dust is mixed and transported vertically by convective systems to high  
20 altitudes (6 km). At the surface, the limit of the southern extension of the extinction  
21 coefficient ( $> 0.06 \text{ km}^{-1}$ ) marks the position of the ITCZ. This limit varies between 2°N in  
22 winter and 15° N in summer.

## 23 **4. Comparison and evaluation**

### 24 **4.1 Comparison of simulation outputs to Aqua-MODIS observations**

1 Figure 10 shows the Level-3 monthly AOTs derived from the combination of the Dark Target  
2 and Deep Blue products (MYD08\_D3.051, MODIS-Aqua Ver. 5.1) at  $1\times 1^\circ$  resolution  
3 averaged from 2006 to 2010. The MODIS data shows important dust activity from January to  
4 August. We observe high AOT values, in excess of 0.5, over large portions of North Africa.  
5 The most important dust activity is observed in March. Two maxima exceeding 1 can be  
6 identified for this month. A primary maximum is located over the gulf of Guinea, Nigeria,  
7 Benin and the region of Ouagadougou (south-west of Niger). This maximum is associated  
8 with the southward dust transport, which is very significant in this season. The secondary  
9 maximum is located in the Bodélé depression in Chad and is therefore collocated with the  
10 main area of dust emission.

11 Compared with the simulated AOTs (Figure 7), ALADIN reproduces the monthly horizontal  
12 distribution of AOT well. However, the model gives larger values of AOT than MODIS,  
13 especially in the Sahelian region, central Mauritania and Mali, from March to July. Still, in  
14 the Bodélé Depression, the maximum AOT (0.8 to 1) simulated by ALADIN in March is  
15 underestimated compared with that given by MODIS (1.2 to 1.4) for the same month. Note  
16 that for this region, Kocha et al. (2013) give an estimate of the AOT bias of MODIS of about  
17 + 0.1. Indeed, AQUA and TERRA observe this region between 09:30 and 12:30 UTC and  
18 capture the maximum of dust concentration. Therefore, Kocha et al (2013) conclude that the  
19 overestimation of the AOT values in the MODIS monthly mean product due to the poor  
20 representation of the diurnal cycle of dust is of the order of 0.1, i.e. 17%.

21 Over the gulf of Guinea, ALADIN underestimates the maximum AOT in March, with a value  
22 around 0.7, while the observed value from MODIS exceeds 1. Over the Mediterranean Sea,  
23 large values of AOT (around 0.5) observed by MODIS are obtained in April near the Libyan  
24 coast, while the maxima of AOT (around 0.5) simulated by ALADIN are obtained in July and

1 August, with a localisation in the Eastern Mediterranean. Over the Atlantic Ocean, a good  
2 agreement is obtained between ALADIN simulations and MODIS observations, in terms of  
3 both horizontal distribution and maximum values of AOT.

#### 4 **4.2 Comparison with AERONET measurements**

5 The AOTs simulated by ALADIN have also been compared with the AERONET observations  
6 available in the AMMA database and the MODIS products. Figures 11 and 12 show,  
7 respectively, the average and scatter plot of monthly optical thickness observed by  
8 AERONET and MODIS and simulated by ALADIN from 2006 to 2010 over Banizoumbou,  
9 Cinzana, Soroa, Mbour and Capo Verde.

10 The large values of AOT ( $> 0.6$ ) measured by AERONET are observed from March to June at  
11 the sites of Banizoumbou, Cinzana and Soroa, with a maximum exceeding 0.8 obtained in  
12 March at Cinzana, in April at Banizoumbou and in May at Soroa (Fig. 11). Indeed, these three  
13 stations are located at the same latitude ( $13^\circ$  N) and they mark the southern boundary of the  
14 sources of dust emission. They are affected by dust transport associated with the Harmattan  
15 wind from March to June, which explains the large AOT values in this season. The low AOTs  
16 are observed from November to January, with values around 0.35, corresponding to the low  
17 dust emission activity. In August, the AOTs are also low at Banizoumbou, Cinzana and  
18 Soroa. For this month, the West African monsoon is well established and the air circulation is  
19 upturned, driving dust aerosol towards the north. A comparison between MODIS and  
20 ALADIN shows that the variations in the averaged monthly AOT are well correlated between  
21 the two datasets, but there are noticeable differences in terms of quantification. For instance,  
22 over Banizoumbou, MODIS observations are slightly larger than AERONET observations for  
23 all months, with a maximum of about 1 observed in April. This overestimation is particularly  
24 perceptible in the wet monsoon season (July and August). For this site, the MODIS data

1 provides a good correlation coefficient (0.864) (Fig. 12). For ALADIN, the maximum of  
2 AOT is given in March with a rather large value of about 1.2. ALADIN overestimates the  
3 AOTs from November to March, and underestimates them from April to September, except  
4 for July. For Banizoumbou, a lower correlation coefficient (0.285) is obtained with ALADIN  
5 compared with MODIS. This weak correlation is probably due to the resolution of the  
6 ALADIN model, which is believed to be too small to provide an appropriate accurate  
7 representation of the surface parameters for this region.

8 Over Cinzana, MODIS gives two maxima of AOT reaching 0.8. The first maximum is  
9 obtained in April and the second in July. The MODIS AOTs are much larger than the  
10 AERONET and ALADIN values, from May to August. The correlation coefficient obtained  
11 for MODIS for Cinzana is about 0.549. In contrast, ALADIN simulates the maximum of AOT  
12 in March (~1) with a correlation coefficient of about 0.418.

13 Over Soroa, the maximum AOT (~0.8) is observed by MODIS in July during the wet West  
14 African monsoon. MODIS overestimates the AOTs from July to March and underestimates  
15 them in May and June compared to AERONET. The correlation coefficient of MODIS is  
16 around 0.128. For Soroa, the AOTs simulated by ALADIN are larger than 0.5 from January to  
17 July, with a maximum of about 1.1 in March. The correlation coefficient obtained for  
18 ALADIN is around 0.255.

19 At Mbour, the maximum AOT measured by AERONET is obtained in June and is around 0.7.  
20 For this site, MODIS values of AOT are larger than AERONET values from January to  
21 August. In July, the AOTs observed by MODIS (0.9) are twice as large as those measured by  
22 AERONET. Like MODIS, ALADIN overestimates the AOTs from January to July, with a  
23 maximum simulated in March (0.8). For Mbour, the correlation coefficients obtained for  
24 MODIS and ALADIN with respect to AERONET are equal to 0.568 and 0.478, respectively.



1 Over Capo Verde, the averaged monthly AOTs observed by AERONET and MODIS, and  
2 simulated by ALADIN, are in good agreement, except in July, where ALADIN overestimates  
3 the AOTs. The maximum AOTs observed and simulated are obtained in July and are equal to  
4 0.5 for AERONET and MODIS and 0.8 for ALADIN. For this site the correlation coefficients  
5 observed for MODIS and ALADIN are 0.603 and 0.584, respectively.

### 6 **4.3 Comparison to surface dust concentration measurements**

7 In this section we use the measured dust mass concentration PM<sub>10</sub> from the SDT  
8 (Marticorena et al., 2010) to evaluate the simulated surface dust concentration from 2006 to  
9 2010. PM<sub>10</sub> measurements refer to particulate matter which passes through a size-selective  
10 inlet with a 50% efficiency cutoff at 10  $\mu\text{m}$  aerodynamic diameter. Therefore, for the  
11 simulated concentrations, we consider only the particles smaller than 10  $\mu\text{m}$  in order to  
12 perform a consistent comparison with the observations. Note that the simulated mass  
13 concentration of particles of less than 10  $\mu\text{m}$  in diameter represents 40.124% of the total  
14 mass.

15 The SDT is composed of three stations, namely Banizoumbou, Cinzana and M'bour. Figure  
16 13 and 14 show, respectively, the monthly mean of the daily median value of measured and  
17 simulated surface concentrations and the scatter plot of monthly ALADIN dust surface  
18 concentration against observations over Banizoumbou, Cinzana and Mbour. The analysis of  
19 this figure shows that the temporal pattern of simulated and observed concentrations is similar  
20 for the Cinzana and Mbour sites, with high concentrations from November to May. In  
21 summer, the simulated and observed surface concentrations are low for these two stations. In  
22 contrast, noticeable differences are seen from April to June at Banizoumbou. For this site, the  
23 simulated surface concentration decreases while the PM<sub>10</sub> concentration remains high. The  
24 model underestimations observed during April to June are probably related to local dust

1 uprisings that are not well simulated by ALADIN model. This underestimation is strong in  
2 June, which marks the transition between the dry and the wet season monsoon in West Africa.  
3 Recently, a study realized by Kocha et al., (2013) shows the existence of two important  
4 processes responsible for dust uprising in West Africa, namely: (1) the diurnal variation of  
5 surface wind speed modulated by the low level jet occurred after sunrise due to turbulent  
6 mixing (Washington et al., 2006), especially in Bodélé depression; (2) the gust wind  
7 associated with the density currents emanating from convective systems occurred at the  
8 afternoon. This second phenomenon generate a strong gust winds can lead to the "dust wall"  
9 known "haboob" (Tulet et al., (2010) ; Knippertz et al. (2012)). We also noted a bias for the  
10 values of AOT in the same period but with a less pronounced intensity than for surface  
11 concentration.

12 In terms of intensity, ALADIN overestimates the monthly surface concentration over  
13 Banizoumbou from November to February. Nevertheless, it underestimates it from April to  
14 July. ALADIN simulates the maximum concentration in March ( $373 \mu\text{g.m}^{-3}$ ) which is in good  
15 agreement with the maximum PM10 observation ( $370 \mu\text{g.m}^{-3}$ ) registered during the same  
16 period. The minimum simulated surface concentration ( $31 \mu\text{g.m}^{-3}$ ) is obtained in September  
17 but the minimum PM10 concentration ( $21 \mu\text{g.m}^{-3}$ ) is observed in August. The square of the  
18 correlation coefficient registered for Banizoumbou is equal 0.473 with a slop of the tendency  
19 curve equal 0.722. Over Cinzana, a good correlation is obtained between the monthly  
20 simulated surface concentration and the PM10 observation, especially from March to  
21 October. The maximum simulated surface concentration and observation is obtained in March  
22 ( $278 \mu\text{g.m}^{-3}$  for ALADIN and  $257 \mu\text{g.m}^{-3}$  for PM10). The minimum surface concentration ( $25$   
23  $\mu\text{g.m}^{-3}$ ) is simulated in September, and the minimum PM10 concentration ( $15 \mu\text{g.m}^{-3}$ ) is  
24 observed in August. For this site, the correlation coefficient and the slope of the tendency  
25 curve are equal 0.648 and 0.894, respectively. Over Mbour, the monthly simulated surface

1 concentrations are larger than the observations over all months except in July and August with  
2 a slope of tendency curve exceeds 1.566. ALADIN simulates the maximum concentration in  
3 January ( $299 \mu\text{g.m}^{-3}$ ) but the maximum PM10 is observed in March ( $202 \mu\text{g.m}^{-3}$ ). The  
4 minimum surface concentration ( $23 \mu\text{g.m}^{-3}$ ) is simulated in August and the minimum PM10  
5 concentration ( $39 \mu\text{g.m}^{-3}$ ) is observed in September. The correlation coefficient obtained over  
6 Mbour is equal 0.804.

7 It is worth mentioning that the dust surface concentration is strongly linked with the surface  
8 dust emission activity. Thus, the largest values for surface concentrations are registered in  
9 spring and winter, which correspond to the period of strong dust emission activity in the  
10 Sahelian region.

#### 11 **4.4 Comparison to CALIOP observations**

12 In this section we use the CALIOP Level 2 Layer version 3.01 product (Koffi et al., 2012)  
13 over the 2007-2009 period to evaluate the ALADIN vertical distribution of dust aerosols.  
14 This data was previously used in Koffi et al. 2012 to evaluate the 12 AeroCom-I (Aerosol  
15 Comparison between observations and models, phase I) models over 13 sub-continental  
16 regions. In this study, the ALADIN-CALIOP intercomparison was limited to the North Africa  
17 (NAF) and Central Africa (CAF) regions. Note that the ALADIN model domain does not  
18 completely cover these two regions. Therefore, in our case, these two regions are defined as  
19 follows:  $[2^{\circ}\text{N}-15^{\circ}\text{N} ; 18^{\circ}\text{W}-48^{\circ}\text{E}]$  for CAF and  $[15^{\circ}\text{N}-35^{\circ}\text{N} ; 18^{\circ}\text{W}-48^{\circ}\text{E}]$  for NAF for  
20 ALADIN. For CALIOP, the same regions as those defined by Koffi et al. (2012) are used:  
21  $[0^{\circ}\text{N}-15^{\circ}\text{N} ; 18^{\circ}\text{W}-60^{\circ}\text{E}]$  for CAF and  $[15^{\circ}\text{N}-35^{\circ}\text{N} ; 18^{\circ}\text{W}-60^{\circ}\text{E}]$  for NAF. The seasonal dust  
22 aerosol mean extinction profiles from CALIOP observations (at 532) from January 2007 to  
23 December 2009 over these two regions are available at  
24 [http://aerocom.met.no/download/CALIOP\\_BENCHMARK\\_KOFFI2012/](http://aerocom.met.no/download/CALIOP_BENCHMARK_KOFFI2012/).

1 Following Koffi et al. (2012), we calculate the mean extinction height  $Z_\alpha$  over the lowest 10  
2 km of the atmosphere in order to assess ALADIN's ability to reproduce the mean vertical  
3 distribution of dust aerosols over CAF and NAF. The following formula is used for  
4 computing  $Z_\alpha$ :

$$5 \quad Z_\alpha = \frac{\sum_{i=1}^n b_{ext,i} \cdot Z_i}{\sum_{i=1}^n b_{ext,i}} \quad (1)$$

6 With  $b_{ext,i}$  the aerosol extinction coefficient ( $\text{km}^{-1}$ ) at level  $i$ , and  $Z_i$  the altitude (km) of level  $i$ .  
7 The sums apply to the first 10 km of the atmosphere.

8 Figure 15 shows the CALIOP and ALADIN mean seasonal extinction coefficient profiles for  
9 NAF. The analysis of the CALIOP measurements allows the seasonal variability of the dust  
10 aerosols profile over NAF to be assessed. In winter, large values for dust aerosol extinction  
11 coefficients are observed between the ground and 2 km of height, which lead to values of  $Z_\alpha$   
12 of about 1.23 km. In spring and summer, the vertical mixing and the activity of sandstorms  
13 are at their maximum. Thus, in summer,  $Z_\alpha$  (2.44 km) is twice as large as in winter. In  
14 autumn, the decrease in dust activity is reflected by a value of  $Z_\alpha$  equal to about 1.85 km.

15 This seasonality also exists for the CAF region (Fig. 16). The maximum of  $Z_\alpha$  is obtained in  
16 June-July-August (2.39 km), with a bimodal vertical distribution. The second peak is located  
17 at around 3.5 km of height. Koffi et al. (2012) explain this feature by the long-range transport  
18 of mineral dust from the Sahara and Sahel regions and the cross-hemispheric transport of  
19 biomass burning products from South Africa, which contribute to the aerosol load in the free  
20 troposphere.

21 Over the NAF region, the ALADIN model reproduces both the shape and the seasonality of  
22 the extinction coefficient profiles rather well. Note that in spring, ALADIN overestimates the  
23 extinction coefficient in the first 2 km. At the surface, ALADIN simulates a peak of about

1 0.18 km<sup>-1</sup>, while the value measured by CALIOP does not exceed 0.11 km<sup>-1</sup>. Above 6 km of  
2 altitude, ALADIN overestimates the extinction coefficient for all seasons. ALADIN  
3 underestimates  $Z_{\alpha}$ , over all seasons in the NAF region, with a maximum of  $Z_{\alpha}$  (1.75 km)  
4 simulated in summer, in accordance with the CALIOP data.

5 Over the CAF region, significant differences are observed in the shape of the CALIOP and  
6 ALADIN extinction profiles. In winter, large extinction coefficient values ( $>0.2$  km<sup>-1</sup>) are  
7 simulated by ALADIN in the first 1 km. This is in connection with the overestimation of  
8 surface dust concentration by ALADIN in this region. Note that the three measurement sites  
9 of dust concentration investigated in section 4.3 (Banizoumbou, Cinzana and Mbour) are  
10 located in this region. In summer and autumn, ALADIN greatly underestimates the extinction  
11 coefficient in the first 5 km. The reason here is that, in addition to dust aerosol, the CALIOP  
12 measurements are affected by other aerosols, such as biomass-burning products, which  
13 contribute to an increase of the extinction coefficient. Note that the  $Z_{\alpha}$  values simulated by  
14 ALADIN are underestimated for all seasons over the CAF region.

## 15 **5. Conclusion**

16 This study focuses on the elaboration and interpretation of a dust aerosol climatology for  
17 North Africa using an operational numerical weather prediction model. The use of a NWP  
18 model for this type of study is novel and allows a better representation of the coupled  
19 processes between the surface and the atmosphere (emission by density currents, topographic  
20 forcing), and the mesoscale processes. The simulated climatology enables us to assess the  
21 location of the main areas of dust emission, dry and wet deposition, and provides a three-  
22 dimensional distribution of monthly dust aerosol optical properties over this region.

23 Results of five-year simulations for the 2006-2010 period are presented. The annual dust  
24 emission in North Africa estimated by ALADIN is about 878 Tg.year<sup>-1</sup>. The Bodélé

1 depression appears as the most important dust source region in North Africa with a total  
2 annual emission of  $21.4 \text{ Tg}\cdot\text{year}^{-1}$ . Dust emission over North Africa is characterized by strong  
3 seasonal variability. The emission is important in spring (296 Tg) and summer (233 Tg), and  
4 drops in winter and autumn to about 196 Tg and 150 Tg, respectively.

5 The principal dry deposition areas are located near dust source emissions. Thus, in the Bodélé  
6 Depression, the mass of dry dust deposition corresponds to about half of the annual dust  
7 emission ( $400\text{-}800 \text{ g}\cdot\text{m}^{-2}\cdot\text{year}^{-1}$ ). The southern limit of the dry deposition area is modulated by  
8 the position of the ITCZ. In winter, the extension of the dry deposition areas is very  
9 significant, especially towards the south and west of Sahara. In summer, the southern limit of  
10 the area of dust deposition is located around  $15^\circ\text{N}$ , in connection with the establishment of the  
11 West African monsoon. The major wet deposition regions depend mainly on the distribution  
12 of large scale and convective precipitation and the direction of dust plume transport. They are  
13 located in the southern part of North Africa (Sahel, Gulf of Guinea, Central Africa and the  
14 Atlantic Ocean). In winter, the wet deposition is very active ( $10$  to  $60 \text{ g}\cdot\text{m}^{-2}$ ) in the band from  
15  $2^\circ$  to  $10^\circ\text{N}$  over the Gulf of Guinea and the Atlantic Ocean. In spring, wet deposition does not  
16 exceed  $40 \text{ g}\cdot\text{m}^{-2}$  over all of North Africa. In summer, wet deposition is very active, with a  
17 maximum simulated over the Bodélé depression and southern Niger ( $140 \text{ g}\cdot\text{m}^{-2}$ ). These  
18 findings are consistent with the existence of large convective systems over the Sahelian  
19 regions in this season.

20 The simulated seasonal cycle of the AOT is in good agreement with MODIS observations.  
21 ALADIN generates prominent features of geographical patterns and seasonal variations that  
22 are in good agreement with the observations. The monthly climatology of AOT presented in  
23 this paper is characterized by two maxima of AOT exceeding 1.2. The first is simulated over

1 the Sahel in March and the second in Mauritania and Mali in July. Low AOTs are simulated  
2 in autumn, again in accordance with MODIS observations.

3 The vertical distribution of dust aerosol is characterized by a large concentration of dust  
4 aerosol at low levels between 0 to 100 m. The maximum of the extinction coefficient is  
5 simulated in March.

6 The comparison of the simulated AOTs with ground AERONET measurements generally  
7 shows a good correlation at a remote site (Capo Verde). However, an overestimation of AOTs  
8 is observed in winter at sites located in the vicinity of dust source regions (Banizoumbou,  
9 Cinzana and Soroa). This overestimation suggests that the content of atmospheric dust is also  
10 overestimated in these source areas in winter. There are two possible reasons here: either the  
11 ALADIN model overestimates dust emission, or it underestimates the removal processes. In  
12 the first case, a possibly overly large emission may be due to an overly low threshold friction  
13 velocity simulated by the ALADIN model, so that the mobilization occurs at an overly low  
14 wind speed.

15 ALADIN simulates the temporal pattern of monthly surface concentrations well, but  
16 overestimates them from late autumn to late winter at all sites. As for the extinction  
17 coefficients, ALADIN reproduces both the shape and the seasonal variability of extinction  
18 coefficient profiles well, especially over the NAF region. In contrast, significant differences  
19 between the CALIOP and ALADIN extinction profiles are obtained over the CAF region.  
20 Indeed, this region is affected by salt and biomass-burning products which heavily influence  
21 the extinction coefficients.

22 It is interesting to note that, despite the absence of any data assimilation process for dust  
23 content in ALADIN, the simulations remain overall satisfactorily correlated with  
24 observations. This result suggests that the model, whose initial and lateral boundary

1 conditions are regularly refreshed by the global model ARPEGE, does not generate any  
2 significant drift of dust content over the whole five-year range of the simulations.

3 Furthermore, the model seems able to maintain a correct relative impact of emission and  
4 deposition processes, which is reflected by the realistic characteristics of the predicted AOT  
5 fields.

6 In future, ALADIN's ability to simulate the dust aerosol content over the Mediterranean Sea  
7 will be investigated. For this purpose, the model will be tested within the framework of the  
8 ChArMeX programme (<http://mistrals.sedoo.fr/ChArMEx>) over the Mediterranean basin and  
9 will be compared with regional climate models over this region.

## 10 **Acknowledgements**

11 This paper is dedicated to the memory of Laurent Gomes.

12 Based on a French initiative, AMMA was built by an international scientific group and is  
13 currently funded by a large number of agencies, especially from France, United Kingdom,  
14 USA and Africa. It has been the beneficiary of a major financial contribution from the  
15 European Community's Sixth Framework Research Programme. Detailed information on  
16 scientific co-ordination and funding is available on the AMMA International web site  
17 <http://www.amma-international.org>. We also acknowledge the MODIS mission scientists and  
18 associated NASA personnel for the production of the data used in this research effort. This  
19 work was supported by the Algerian Met Office (ONM), Météo France, Centre National de  
20 Recherches Météorologiques (CNRM) and the French Embassy in Algeria.

## 21 **References**

22 Albrecht, B. A.: Aerosols, cloud microphysics, and fractional cloudiness, *Science*, 245, 1227–  
23 1230, 1989.



1 Al Saadi, J., Szykman, J., Pierce, R. B., Kittaka, C., Neil, D., Chu, D. A., Remer, L. A.,  
2 Gumley, L., Prins, E., Weinstock, L., MacDonald, C., Wayland, R., Dimmick, F., and  
3 Fishman, J.: Improving national air quality forecasts with satellite aerosol observations, *Bull.*  
4 *Am. Meteorol. Soc.*, 1249–1261, doi:10.1175/BAMS-86-9-1249, 2005.

5 Bagnold, R. A.: *The Physics of Blown Sand and Desert Dunes*, 265 pp, Methuen, New York,  
6 1941.

7 Bechtold, P., Bazile, E., Guichard, F., Mascart, P., and Richard, E.: A Mass flux convection  
8 scheme for regional and global models, *Q. J. R. Meteorol. Soc.* 127, 869-886, 2001.

9 Binkowski, F. S., and Roselle, S.: Models-3 community multiscale air quality (cmaq) model  
10 aerosol component 1, model description, *J. Geophys Res.* 108(D6), 4183, doi :  
11 10.1029/2001JD001409, 2003.

12 Bougeault, P.: A simple parameterization of the large-scale effects of cumulus convection,  
13 *MWR*, 113, 2108–2121, 1985.

14 Bougeault, P., and Lacarrère, P.: Parameterization of orography-induced turbulence in a  
15 mesobeta-scale model, *Mon. Wea. Rev.* 117, 1872–1890, 1989.

16 Bouteloup, Y., Bouyssel, F., and Marquet, P. : Improvements of Lopez's prognostic large scale  
17 cloud and precipitation scheme, *ALADIN Newsletter*. 28, p.66-73, 2005.

18 Bréon, F.M., Vermeulen, A., and Descloitres, J.: An evaluation of satellite aerosol products  
19 against sunphotometers measurements, *Remote Sens. Environ.* 115, 3102–3111,  
20 doi:10.1016/j.rse.2011.06.017, 2011.

21 Brooks, N. P., and Legrand, M.: Dust variability over Northern Africa and rainfall in Sahel, in  
22 *linking the climate change to landsurface change*, Kluwer Academic Publishers, Dordrecht,  
23 Netherlands, 1–25 pp, 2000.

1 Bubnová, R., Hello, G., Bénard, P., and Geleyn, J. F.: Integration of the fully elastic equations  
2 cast in the hydrostatic pressure terrain following coordinate in the framework of the ALADIN  
3 NWP system, *Mon. Wea. Rev.* 123, 515–535, 1995.

4 Callot, Y., Marticorena, B., and Bergametti, G.: Geomorphologic approach for modelling the  
5 surface features of arid environments in a model of dust emission: application to the Sahara  
6 desert, *Geodinamica Acta* 13 245-270, 2000.

7 Catry, B., Geleyn, J.F., Bouyssel, F., Cedilnik, J., Brozkova, R., Derkova, M., Mladek, R.: A  
8 new sub-grid scale lift formulation in a mountain drag parameterisation scheme,  
9 *Meteorologische Zeitschrift*. 17, Issue 2, 193-208, 2008.

10 Chepil, W. S.: Properties of soil which influence wind erosion: IV. State or dry aggregate  
11 structure, *Soil Sci.* 72, 387-401, 1951.

12 Chin, M., Jacob, D. J., Gardner, G. M., Foreman-Fowler, M.S., Spiro, P.A., and Savoie, D. L.:  
13 A global three-dimensional model of tropospheric sulfate, *J. Geophys. Res.*101, 18667–  
14 18690, doi:10.1029/96JD01221, 1996.

15 Crumeyrolle, S., Gomes, L., Tulet, P., Matsuki, A., Schwarzenboeck, A., and Crahan, K.:  
16 Increase of the aerosol hygroscopicity by cloud processing in a mesoscale convective system:  
17 a case study from the AMMA campaign, *Atmos. Chem. Phys.*, 8, 6907–6924,  
18 doi:10.5194/acp-8-6907-2008, 2008.

19 Crumeyrolle, S., Tulet, P., Gomes, L., Garcia-Carreras, L., Flamant, C., Parker, D. J.,  
20 Matsuki, A., Formenti, P., and Schwarzenboeck, A.: Transport of dust particles from the  
21 Bodélé region to the monsoon layer- AMMA case study of the 9-14 June 2006 period, *Atmos.*  
22 *Chem. Phys.* 11, 479-494, doi:10.5194/acp-11-479-2011, 2011.

23 Cuxart, J., Bougeault, P., and Redelsperger, J.L.: A turbulence scheme allowing for mesoscale  
24 and large-eddy simulations, *Q. J. R. Meteorol. Soc.* 126, p.1-30, 2000.

1 d'Almeida, G. A.: A model for Saharan dust transport, *J. Clim. Appl. Meteorol.* 25, 903-916,  
2 1986.

3 Dirksen, R. J., Boersma, K. F., de Laat, J., Stammes, P., van der Werf, G. R., Val Martin, M.,  
4 and Kelder, H. M.: An aerosol boomerang: rapid around-the-world transport of smoke from  
5 the December 2006 Australian forest fires observed from space, *J. Geophys. Res.*, 114,  
6 D21201, doi:10.1029/2009JD012360, 2009.

7 Engel-Cox, J. A., Hoff, R. M., Rogers, R., Dimmick, F., Rush, A. C., Szykman, J. J., Al-  
8 Saadi, J., Chu, D. A., and Zell, E. R.: Integrating LIDAR and satellite optical depth with  
9 ambient monitoring for 3-D dimensional particulate characterization, *Atmos. Environ.*, 40,  
10 8056–8067, 2006.

11 Engelstaedter, S., Tegen, I., and Washington, R.: North African dust emissions and transport,  
12 *Earth-Sci. Rev.* 79, 73-100, 2006.

13 Flamant, C., Chaboureau, J-P., Parker, D. J., Taylor, C. M., Cammas, J-P., Bock, O., Timouk,  
14 P., and Pelon, J.: Airborne observations of the impact of a convective system on the planetary  
15 boundary layer thermodynamics and aerosol distribution in the intertropical discontinuity  
16 region of the West African monsoon, *Q. J. R. Meteorol. Soc.* 133, 1–28, 2007.

17 Fouquart, Y., and Bonnel, B.: Computations of solar heating of the earth's atmosphere: a new  
18 parameterization, *Beitr. Phys. Atmosph.* 53, 35-62, 1980.

19 Ginoux, P., Prospero, J.M., Torres, O., and Chin, M.: Long-term simulation of global dust  
20 distribution with the GOCART model: correlation with North Atlantic Oscillation, *Environ.*  
21 *Model. Software*, 19, 113–128, 2004.

22 Grini, A., Tulet, P., and Gomes, L.: Dusty weather forecasts using the MesoNH mesoscale  
23 atmospheric model, *J. Geophys. Res.* VOL. 111, D19205, doi:10.1029/2005JD007007, 2006.

1 Haywood, J.M., Francis, P.N., Glew, M.D., Taylor, J.P.: Optical properties and direct  
2 radiative effect of Saharan dust: a case study of two Saharan dust outbreaks using aircraft  
3 data. *J. Geophys. Res. Atmospheres*, 106 (D16), 18,417– 18,430, 2001.

4 Holben, B. N., Eck, T. F., Slutsker, I., Tanré, D., Buis, J. P., Setzer, A., Vermote, E., Reagan,  
5 J. A., Kaufman, Y., Nakajima, T., Lavenu, F., Jankowiak, I., and Smirnov, A.: AERONET-A  
6 Federated Instrument Network and Data Archive for Aerosol Characterization, *Remote Sens.*  
7 *Environ.* 66, 1–16, doi:10.1016/S0034-4257(98)00031-5, 1998.

8 Holben, B. N., Tanre, D., Smirnov, A., Eck, T. F., Slutsker, I., Abuhassan, N., Newcomb, W.  
9 W., Schafer, J., Chatenet, B., Lavenu, F., Kaufman, Y., Van de Castle, J., Setzer, A.,  
10 Markham, B., Clark, D., Frouin, R., Halthore, R., Karnieli, A., O’Neill, N. T., Pietras, C.,  
11 Pinker, R. T., Voss, K., and Zibordi, G.: An emerging ground-based aerosol climatology:  
12 Aerosol Optical Depth from AERONET, *J. Geophys. Res.*, 106, 12067–12098, 2001.

13 Houghton, J., Ding, Y., Griggs, D.J., Noguier, M., Vander Linden, P.J., Dai, X., Maskell, K.,  
14 Johnon, C.A.: *Climate Change 2001: The Scientific Basis*. Cambridge University Press. New  
15 York, 2001.

16 Hsu, N. C., Tsay, S.C., King, M., and Herman, J. R.: Aerosol properties over bright-reflecting  
17 source regions, *IEEE. T. Geosci. Remote*, 42, 557–569, doi: 10.1109/TGRS.2004.824067,  
18 2004.

19 Hsu, N. C., Tsay, S., King, M. D., and Herman, J. R.: Deep Blue Retrievals of Asian Aerosol  
20 Properties During ACE-Asia, *IEEE T. Geosci. Remote*, 44, 3180–3195, 2006.

21 Hunt, W. H., Winker, D. M., Vaughan, M. A., Powell, K. A., Lucker, P. L., and Weimer, C.:  
22 CALIPSO lidar description and performance assessment, *J. Atmos. Ocean. Tech.*, 26, 1214–  
23 1228, doi:10.1175/2009jtecha1223.1, 2009.

24 Intergovernmental Panel on Climate Control (IPCC): *Climate Change 2007: The Physical*  
25 *Basis*, in: *Changes in Atmospheric Constituents and in Radiative Forcing*, the Fourth,

1 Assessment Report of the IPCC, edited by: Forster, P., Ramaswamy, V., Artaxo, R., Berntsen,  
2 T., Betts, R., Fahey, D. W., Haywood, J., Lean, J., Lowe, D. C., Myhre, G., Nganga, J., Prinn,  
3 R., Raga, G., Schulz, M., and Van Dorland, R.: Cambridge University Press. Cambridge, UK  
4 and New York, NY, USA, pp. 129-234, 2007.

5 Intergovernmental Panel on Climate Change (IPCC): Climate Change 2013: The Physical  
6 Science Basis in: Clouds and Aerosols, Contribution of Working Group I to the Fifth  
7 Assessment Report of the Intergovernmental Panel on Climate Change [Stocker, T.F., D.  
8 Qin, G.-K. Plattner, M. Tignor, S.K. Allen, J. Boschung, A. Nauels, Y. Xia, V. Bex and P.M.  
9 Midgley (eds.)], Boucher, O., D. Randall, P. Artaxo, C. Bretherton, G. Feingold, P. Forster,  
10 V.-M. Kerminen, Y. Kondo, H. Liao, U. Lohmann, P. Rasch, S.K. Satheesh, S. Sherwood, B.  
11 Stevens and X.Y. Zhang, Cambridge University Press, Cambridge, United Kingdom and New  
12 York, NY, USA, 1535 pp, doi:10.1017/CBO9781107415324, 2013.

13 Kaufman, Y. J., Koren, I., Remer, L.A., Tanré, D., Ginoux, P., and Fan, S.: Dust transport and  
14 deposition observed from the Terra-Moderate Resolution Imaging Spectroradiometer  
15 (MODIS) spacecraft over the Atlantic Ocean, *J. Geophys. Res.* 110, D10S12,  
16 doi:10.1029/2003JD004436, 2005.

17 Kinne, S., Schulz, M., Textor, C., Guibert, S., Balkanski, Y., Bauer, S. E., Berntsen, T.,  
18 Berglen, T. F., Boucher, O., Chin, M., Collins, W., Dentener, F., Diehl, T., Easter, R.,  
19 Feichter, J., Fillmore, D., Ghan, S., Ginoux, P., Gong, S., Grini, A., Hendricks, J., Herzog, M.,  
20 Horowitz, L., Isaksen, I., Iversen, T., Kirkevåg, A., Kloster, S., Koch, D., Kristjansson, J. E.,  
21 Krol, M., Lauer, A., Lamarque, J. F., Lesins, G., Liu, X., Lohmann, U., Montanaro, V.,  
22 Myhre, G., Penner, J., Pitari, G., Reddy, S., Seland, O., Stier, P., Takemura, T., and Tie, X.:  
23 An AeroCom initial assessment – optical properties in aerosol component modules of global  
24 models, *Atmos. Chem. Phys.* 6. 1815-1834, doi:10.5194/acp-6-1815-2006, 2006.

1 Kinne, S., O'Donnel, D., Stier, P., Kloster, S., Zhang, K., Schmidt, H., Rast, S., Giorgetta, M.,  
2 Eck, T.F., and Stevens, B.: MAC-v1: A new global aerosol climatology for climate studies, *J.*  
3 *Adv. Model. Earth Syst.* 5. 704–740, doi:10.1002/jame.20035, 2013.

4 Knippertz P., and Todd, M. C., Mineral dust aerosols over the Sahara: Meteorological  
5 controls on emission and transport and implications for modeling, *Rev. Geophys.*, 50,  
6 RG1007, doi:10.1029/2011RG000362, 2012.

7 Kocha, C., Lafore, J.P., Tulet, P., and Seity, Y.: High resolution simulation of a major West  
8 African dust storm: Comparison with observations and investigation of dust impact, *Q. J. R.*  
9 *Meteorol. Soc.* 138, 455-470, doi:10.1002/qj.927, 2012.

10 Kocha, C., Tulet, P., Lafore, J.P., and Flamant, C.: The importance of the diurnal cycle of  
11 Aerosol Optical Depth in West Africa, *Geophys. Res. Lett.* 40, doi:10.1002/grl.50143, 2013.

12 Koffi, B., Schulz, M., Bréon, F-M., Griesfeller, J., Winker, D.M.M., Balkanski, Y., Bauer, S.,  
13 Berntsen, T., Chin, M., Collins, W.D., Dentener, F., Diehl, T., Easter, R.C., Ghan, S.J.,  
14 Ginoux, P.A., Gong, S., Horowitz, L.W., Iversen, T., Kirkevåg, A., Koch, D.M., Krol, M.,  
15 Myhre, G., Stier, P., and Takemura, T.: Application of the CALIOP Layer Product to evaluate  
16 the vertical distribution of aerosols estimated by global models: Part 1. AeroCom phase I  
17 results, *J. Geophys. Res.* 117, no. D10, D10201, doi:10.1029/2011JD016858, 2012.

18 Laurent, B., Marticorena, B., Bergametti, G., Léon, J.F., and Mahowald, N.M.: Modeling  
19 mineral dust emissions from the Sahara desert using new surface properties and soil database.  
20 *J. Geophys. Res.* 113, D14218, doi:10.1029/2007JD009484, 2008.

21 Levy. R. C., Remer, L. A., Mattoo, S., Vermote, E. F., and Kaufman, Y. J.: Second-  
22 generation operational algorithm: Retrieval of aerosol properties over land from inversion of  
23 Moderate Resolu-tion Imaging Spectroradiometer spectral reflectance, *J. Geophys. Res.*, 112,  
24 D13211, doi: 10.1029/2006JD007811, 2007.

1 Levy, R. C., Remer, L. A., Kleidman, R. G., Mattoo, S., Ichoku, C., Kahn, R., and Eck, T. F.:  
2 Global evaluation of the Collection 5 MODIS dark-target aerosol products over land, *Atmos.*  
3 *Chem. Phys.*, 10, 10399–10420, doi:10.5194/acp-10-10399-2010, 2010.

4 Levy, R. C., Mattoo, S., Munchak, L. A., Remer, L. A., Sayer, A. M., Patadia, F., and Hsu N.  
5 C.: The Collection 6 MODIS aerosol products over land and ocean, *Atmos. Meas. Tech.*, 6,  
6 2989–3034, doi:10.5194/amt-6-2989-2013, 2013.

7 Liousse, C., Penner, J. E., Chuang, C., Walton, J. J., Eddleman, H., and Cachier, H.: A global  
8 three-dimensional model study of carbonaceous aerosols, *J. Geophys. Res.* 101, 19411–  
9 19432, doi:10.1029/95JD03426,1996.

10 Lopez, P.: Implementation and validation of a new prognostic large-scale cloud and  
11 precipitation scheme for climate and data-assimilation purposes, *Q. J. R. Meteorol. Soc.*, 128,  
12 229-257, 2002.

13 Luo, C., Mahowald, N.M., and del Corral, J.: Sensitivity study of meteorological parameters  
14 on mineral aerosol mobilization, transport, and distribution, *J. Geophys. Res.* 108, 4447,  
15 doi:10.1029/2003JD003483, 2003.

16 Mallet, M., Tulet, P., Serc, D., Solmon, F., Dubovik, O., Pelon, J., Pont, V., and Thouron, O.:  
17 Impact of dust aerosols on the radiative budget, surface heat fluxes, heating rate profiles and  
18 convective activity over West Africa during March 2006, *Atmos. Chem. Phys.*, 9, 7143–7160,  
19 doi:10.5194/acp-9-7143-2009, 2009.

20 Marticorena, B., and Bergametti, G.: Modeling the atmospheric dust cycle: 1. Design of a  
21 soil-derived dust emission scheme, *J. Geophys. Res.* 100, 16, 415-16, 430, 1995.

22 Marticorena, B., and Bergametti, G.: Two year simulations of seasonal and interannual  
23 changes in Saharan dust emissions. *Geophys. Res. Lett.* 23, 1921-1924, 1996.

24 Marticorena, B., Chatenet, B., Rajot, J.L., Traoré, S., Coulibaly, M., Diallo, A., Koné, I.,  
25 Maman, A., NDiaye, T., and Zakou, A.: Temporal variability of mineral dust concentrations

1 over West Africa: analyses of a pluriannual monitoring from the AMMA Sahelian Dust  
2 Transect, *Atmos. Chem. Phys.* 10, 8899-8915, 2010.

3 Martin, J.H.: Iron still comes from above, *Nature* 353, 123, doi:10.1038/353123b0, 1991.

4 Martin, R.V., Jacob, D.J., Yantosca, R.M., Chin, M., and Ginoux, P.: Global and regional de-  
5 creases in tropospheric oxidants from photo-chemical effects of aerosols. *J. Geophys. Res.*  
6 108 (D3), 4097, doi:10.1029/2002JD002622, 2003.

7 Masson, V., Champeaux, J., Chauvin, F., Meriguet, C., and Lacaze, R.: A global database of  
8 land surface parameters at 1-km resolution in meteorological and climate models, *J. Clim.*  
9 1261–1282, 2003.

10 Masson, V., Le Moigne, P., Martin, E., Faroux, S., Alias, A., Alkama, R., Belamari, S.,  
11 Barbu, A., Boone, A., Bouysse, F., Brousseau, P., Brun, E., Calvet, J.C., Carrer, D.,  
12 Decharme, B., Delire, C., Donier, S., Essaouini, K., Gibelin, A.L., Giordani, H., Habets, F.,  
13 Jidane, M., Kerdraon, G., Kourzeneva, E., Lafaysse, M., Lafont, S., Lebeaupin Brossier, C.,  
14 Lemonsu, A., Mahfouf, J.F., Marguinaud, P., Mokhtari, M., Morin, S., Pigeon, G., Salgado,  
15 R., Seity, Y., Taillefer, F., Tanguy, G., Tulet, P., Vincendon, B., Vionnet, V., and Voldoire,  
16 A.: The SURFEXv7.2 land and ocean surface platform for coupled or offline simulation of  
17 earth surface variables and fluxes, *Geosci. Model Dev.* 6, 929–960, doi:10.5194/gmd-6-929-  
18 2013, 2013.

19 Meloni, D., Sarra, A. D., Di Iorio, T., and Fiocco, G.: Influence of the vertical profile of  
20 Saharan dust on the visible direct radiative forcing, *Journal of Quantitative Spectroscopy and*  
21 *Radiative Transfer*. V. 93, issue 4, p. 397–413, 2005.

22 Mlawer, E. J., Taubman, S. J., Brown, P. D., Iacono, M.J., and Clough, S.A.: RRTM, a  
23 validated correlated-k model for the longwave, *J. Geophys. Res.* 102, 16,663-16,682, 1997.



1 Mokhtari, M., Gomes, L., Tulet, P., and Rezoug, T.: Importance of the surface size  
2 distribution of erodible material: an improvement on the Dust Entrainment And Deposition  
3 (DEAD) Model. *Geosci. Model Dev.* 5, 581–598, doi:10.5194/gmd-5-581-2012, 2012.

4 Morcrette, J.J.: Radiation and cloud radiative properties in the ECMWF operational weather  
5 forecast model. *J. Geophys. Res.* 96D, 9121-9132, 1991.

6 Morcrette, J.J., Boucher, O., Jones, L., Salmond, D., Bechtold, P., Beljaars, A., Benedetti, A.,  
7 Bonet, A., Kaiser, J. W., Razinger, M., Schulz, M., Serrar, S., Simmons, A. J., Sofiev, M.,  
8 Suttie, M., Tompkins, A. M., and Untch, A.: Aerosol analysis and forecast in the European  
9 Centre for Medium-Range Weather Forecasts Integrated Forecast System: Forward modeling.  
10 *J. Geophys. Res.* 11 4, D06206, doi:10.1029/2008JD011235, 2009.

11 Nabat, P., Somot, S., Mallet, M., Chiapello, I., Morcrette, J. J., Solmon, F., Szopa, S., Dulac,  
12 F., Collins, W., Ghan, S., Horowitz, L. W., Lamarque, J. F., Lee, Y. H., Naik, V., Nagashima,  
13 T., Shindell, D., and Skeie, R.: A 4-D climatology (1979–2009) of the monthly tropospheric  
14 aerosol optical Thickness distribution over the Mediterranean region from a comparative  
15 evaluation and blending of remote sensing and model products, *Atmos. Meas. Tech.* 6, 1287–  
16 1314, doi:10.5194/amt-6-1287, 2013.

17 Noilhan, J., And Planton, S.: A simple parameterization of land surface processes for  
18 meteorological models. *Mon. Wea. Rev.* 117, 536-549, 1989.

19 Prospero, J.M., Ginoux, P., Torres, O., Nicholson, S.E., and Gill, T. E.: Environmental  
20 characterization of global sources of atmospheric soil dust identified with the nimbus 7 total  
21 ozone mapping spectrometer (toms) absorbing aerosol product. *Rev. Geophys.* 40,1002,  
22 doi:10.1029/2000RG000095, 2002.

23 Radnóti, G.: Comments on “A spectral limited-area formulation with time-dependent  
24 boundary conditions applied to the shallowwater equations”. *Mon. Wea. Rev.* 123, 3122–  
25 3123, 1995.

1 Remer, L. A., Kaufman, Y. J., Tanré, D., Matoo, S., Chu, D. A., Martins, J. V., Li, R.R.,  
2 Ichoku, C., Levy, R. C., Kieidman, R. G., Eck, T. F., Vermote, E., and Holben, B. N.: The  
3 MODIS Aerosol Algorithm, Products, and Validation, *J. Atmos. Sci.* 62, 947–73,doi:  
4 10.1175/JAS3385.1, 2005.

5 Rodwell, M.: The local and global impact of the recent change in model aerosol climatology.  
6 *ECMWF Newsl*, 105, 17 – 23, 2005.

7 Rogers, R. R., Vaughan, M. A., Hostetler, C. A., Burton, S. P., Ferrare, R. A., Young, S. A.,  
8 Hair, J.W., Obland, M. D., Harper, D. B., Cook, A. L., and Winker, D. M.: Looking through  
9 the haze: evaluating the CALIPSO level 2 aerosol optical depth using airborne high spectral  
10 resolution lidar data, *Atmos. Meas. Tech.*, 7, 4317–4340, doi:10.5194/amt-7-4317-2014,  
11 2014.

12 Sandu, I., Brenguier, J., Geoffroy, O., Thouron, O., and Masson, V.: Aerosol impacts on the  
13 diurnal cycle of marine stratocumulus. *J. Atmos. Sci.* 65, 2705–2718, 2008.

14 Satheesh, S. K.: *Letter to the Editor* Aerosol radiative forcing over land: effect of surface and  
15 cloud reflection, *Ann. Geophys.*, 20, 2105–2109, doi:10.5194/angeo-20-2105-2002, 2002.

16 Schepanski, K., Tegen, I., and Macke, A.: Comparison of satellite based observations of  
17 Saharan dust source areas. *Remote Sensing of Environment*, V.123. 90-97, 2012.

18 Schmechtig, C., Marticorena, B., Chatenet, B., Bergametti, G., Rajot, J. L., and Coman, A.:  
19 Simulation of the mineral dust content over Western Africa from the event to the annual scale  
20 with the CHIMERE-DUST model. *Atmos. Chem. Phys.* 11, 7185–7207, doi:10.5194/acp-11-  
21 7185-2011, 2011.

22 Seinfeld, J. H., and Pandis, S. N.: 1997. *Atmospheric chemistry and physics: From Air*  
23 *Pollution to Climate Change*, John Wiley, New York, pp. 292-293, 1997.

1 Shi, Y., Zhang, J., Reid, J. S., Hyer, E. J., and Hsu, N. C.: Critical evaluation of the MODIS  
2 Deep Blue aerosol optical depth product for data assimilation over North Africa. *Atmos.*  
3 *Meas. Tech.*, 6, 949–969, doi:10.5194/amt-6-949, 2013.

4 Smith R.N.B.: A scheme for predicting layer clouds and their water content in a general  
5 circulation model. *Q. J.R. Meteorol. Soc.* 116, 435-460, 1990.

6 Sokolik, I. N., Winker, D. M., Bergametti, G., Gillette, D. A., Carmichael, G., Kaufman, Y.  
7 J., Gomes, L., Schuetz, L., and Penner, J. E.: Introduction to special section: Outstanding  
8 problems in quantifying the radiative impacts of mineral dust, *J. Geophys. Res.-Atmos.*  
9 106(D16), 18015–18027, 2001.

10 Stephens, G. L., Vane, D. G., Boain, R. J., Mace, G. G., Sassen, K., Wang, Z., Illingworth, A.  
11 J., O'Connor, E. J., Rossow, W. B., Durden, S. L., Miller, S. D., Austin, R. T., Benedetti, A.,  
12 and Mitrescu, C.: The cloudsat mission and the A-Train: a new dimension of space-based  
13 observations of clouds and precipitation, *B. Am. Meteorol. Soc.*, 83, 1771–1790+1742, 2002.

14 Swap, R.M., Garstang, M., Greco, S., Talbot, R., Kallberg, P.: Saharan dust in the Amazon  
15 basin. *Tellus B* 44, 133–149, 1992.

16 Tanaka, T.Y., and Chiba, M.: Global Simulation of Dust Aerosol with a Chemical Transport  
17 Model, MASINGAR. *Journal of the Meteorological Society of Japan* Vol. 83A, pp. 255—  
18 278, 2005.

19 Tanré, D., Geleyn, J.F., and Slingo, J. M.: First results of the introduction of an advanced  
20 aerosol-radiation interaction in the ECMWF low resolution global model, in *Aerosols and*  
21 *Their Climatic Effects*. edited by H. E. Gerber, pp. 133 – 177, A. Deepak, Hampton, Va,  
22 1984.

23 Tanré, D., Kaufman, Y. J., Herman, M., and Mattoo, S.: Remote sensing of aerosol properties  
24 over oceans using the MODIS/EOS spectral radiances, *J. Geophys. Res.* 102, 16971–16988,  
25 1997.

1 Tegen, I., and Fung, I.: Contribution to the atmospheric mineral aerosol load from land  
2 surface modification, *J. Geophys. Res.*, 100, 18707–18726, doi:10.1029/95JD02051, 1995.

3 Tegen, I., Hollrig, P., Chin, M., Fung, I., Jacob, D., and Penner, J.: Contribution of different  
4 aerosol species to the global aerosol extinction optical thickness: Estimates from model  
5 results, *J. Geophys. Res.* 102, 23895–23915, 1997.

6 Todd, M.C., Washington, R., Martins, J.V., Dubovik, O., Lizcano, G., M'Bainayel, S., and  
7 Engelstaedter, S.: Mineral dust emission from the Bodélé Depression, northern Chad, during  
8 BoDEx 2005. *J. Geophys. Res.* 112, D06207, doi:10.1029/2006JD007170, 2007.

9 Tompkins, A M., Cardinali, C., Morcrette, J.J., and Rodwell, M.: Influence of aerosol  
10 climatology on forecasts of the African Easterly Jet, *Geophys. Res. Lett.* 32 , L10801,  
11 doi:10.1029/2004GL022189, 2005.

12 Tost, H., Jöckel, P., Kerkweg, A., Sander, R., and Leliveld, J.: Technical note: A new  
13 comprehensive SCAVenging submodel for global atmospheric chemistry modelling, *Atmos.*  
14 *Chem. Phys.*, 6, 565-574, 2006.

15 Tulet, P., Crassier, V., Cousin, F., Suhre, K., and Rosset, R.: ORILAM, a three-moment  
16 lognormal aerosol scheme for mesoscale atmospheric model: Online coupling into the Meso-  
17 NH-C model and validation on the Escompte campaign, *J. Geophys. Res.* VOL. 110, D18201,  
18 doi:10.1029/2004JD005716, 2005.

19 Tulet, P., Mallet, M., Pont, V., Pelon, J., and Boone, A.: The 7–13 March, 2006, dust storm  
20 over West Africa: generation, transport and vertical stratification, *J. Geophys. Res.*, 113,  
21 D00C08, doi:10.1029/2008JD009871, 2008.

22 Tulet, P., Crahan-Kaku, K., Leriche, M., Aouizerats, B., and Crumeyrolle, S.: 2010. Mixing  
23 of dust aerosols into mesoscale convective system : Generation, filtering and possible  
24 feedbacks on ice anvils, *Atmospheric Research*, 96, 302–314,  
25 doi:10.1016/j.atmosres.2009.09.011, 2010.

1 Twomey, S.: The nuclei of natural cloud formation. II: The supersaturation in natural clouds  
2 and the variation of cloud droplet concentration, *Pure and Applied Geophysics* 43:243-249,  
3 1959.

4 United States Department of Agriculture (USDA), Natural Resources Conservation Service  
5 (NRCS):. *Soil Taxonomy : A Basic System of Soil Classification for Making and Interpreting*  
6 *Soil Surveys Agr. Handb.* 436. U.S.Govt.Print.Office, Washington DC, 20402. Second  
7 edition, 1999.

8 Wang, T., Cheung, T. F., Li, Y. S., Xu, X. M., and Blake, D. R.: Emission characteristics of  
9 CO, NO<sub>x</sub>, SO<sub>2</sub> and indications of biomass burning observed at a rural site in eastern China. *J.*  
10 *Geo-phys. Res.* 107(D12), 4157, doi:10.1029/2001JD000724, 2002.

11 Washington, R., Todd, M., Middleton, N. J., and Goudie, A. S.: Dust-Storm source areas  
12 determined by the total ozone monitoring spectrometer and surface observations, *Annals of*  
13 *the Association of American Geographers.* 93 (2), 297, 2003.

14 Washington, R., Todd, M. C., Engelstaedter, S., Mbainayel, S., and Mitchell, F.: Dust and the  
15 low-level circulation over the Bodélé depression, Chad: Observations from BoDEX 2005, *J.*  
16 *Geophys. Res.*, 111, D03201, doi:10.1029/2005JD006502, 2006.

17 Werner, M., Tegen, I., Harrison, S. P., Kohfeld, K. E., Prentice, I. C., Balkanski, Y., Rodh,  
18 H., and Roelandt, C.: Seasonal and interannual variability of the mineral dust cycle under  
19 present and glacial climate conditions, *J. Geophys. Res.* 107, 4744,  
20 doi:10.1029/2002JD002365, 2002.

21 Winker, D. M., Hunt, W. H., and McGill, M. J.: Initial performance assessment of CALIOP,  
22 *Geophys. Res. Lett.*, 34, L19803, doi:10.1029/2007GL030135, 2007.

23 Zender, C. S., Bian, H., and Newman, D.: Mineral Dust Entrainment and deposition (DEAD)  
24 model: Description and 1990s dust climatology, *J. Geophys. Res.* VOL. 108, NO. D14, 4416,  
25 doi:10.1029/2002JD002775, 2003a.

1 Zhu, A., Ramanathan, V., Li, F., and Kim, D.: Dust plumes over the Pacific, Indian, and  
2 Atlantic oceans: climatology and radiative impact, *J. Geophys. Res.* 112, D16208,  
3 doi:10.1029/2007JD008427, 2007.

4

5

1 **Table 1:** Log-normal parameters of the AMMA size distribution used in DEAD coupled with  
 2 SURFEX.

|  | Mode 1 | Mode 2 | Mode 3 |
|--|--------|--------|--------|
| Number fraction (%)                      | 97.52  | 1.95   | 0.52   |
| Mass fraction (%)                        | 0.08   | 0.92   | 99     |
| Geometric standard deviation             | 1.75   | 1.76   | 1.7    |
| Number median diameter ( $\mu\text{m}$ ) | 0.078  | 0.64   | 5.0    |
| Mass median diameter ( $\mu\text{m}$ )   | 0.2    | 1.67   | 11.6   |

3

1 **Table 2:** Comparison of regional annual mean dust flux between this study and other studies.

2 The unit is Tg.year<sup>-1</sup>.

3

| References                       | Annual mean dust emission<br>(Tg.year <sup>-1</sup> ) in North Africa |                    |
|----------------------------------|---|--------------------|
| This study                       | 878   | period (2006-2010) |
| d'Almeida (1986)                 | 630-710   | period (1981-1982) |
| Luo et al.(2003)                 | 1114  | period (1979-2000) |
| Ginoux et al. (2004)             | 1430  | period (1981-1996) |
| Marticorena et Bergametti (1996) | 665-586   | period (1991-1992) |
| Callot et al. (2000)             | 760   | period (1990-1992) |
| Laurent et al. (2008)            | 580-760   | period (1996-2001) |
| Tanaka and Chiba (2005)          | 1018  | period (1979-2003) |
| Werner et al. (2002)             | 693   | period (1979-1989) |
| Zender et al. (2003a)            | 980   | period (1990-1999) |

4

5



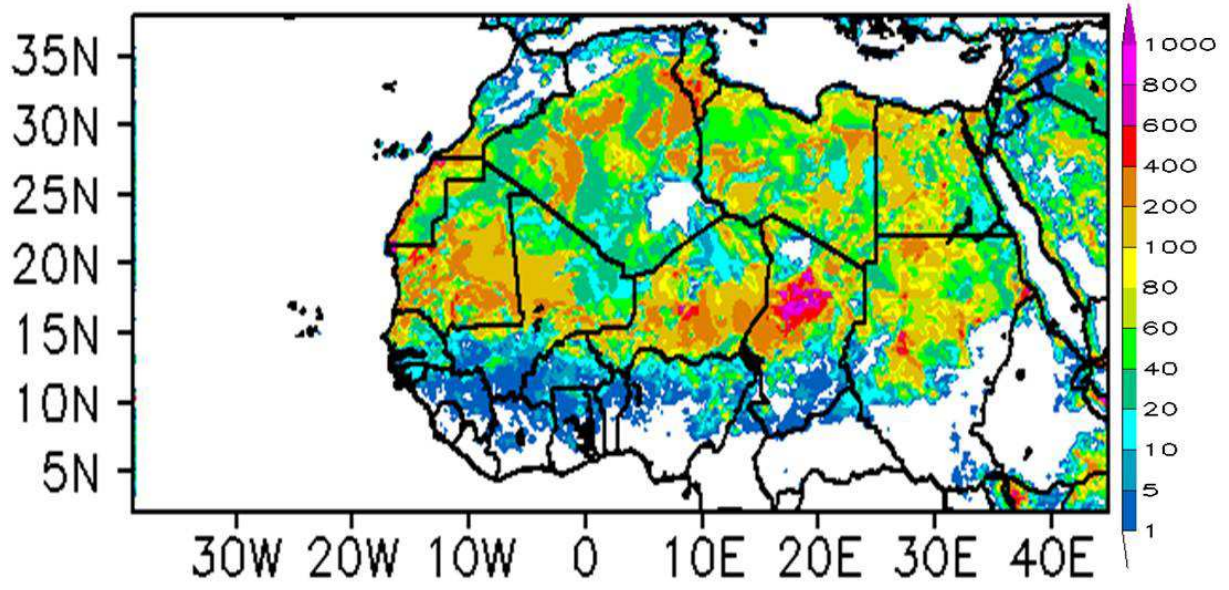
1 **Table 3:** Mean dust wet deposition

| Models              | Wet deposition for 2006 in ( $\text{g.m}^{-2}.\text{year}^{-1}$ ) |
|---------------------|---|
| BSC-DREAM8b         | 0.46  |
| GOCART-v4Ed.A2.CTRL | 9.653   |
| GISS-modelE.A2.CTRL | 8.301   |
| TM5-V3.A2.CTRL      | 4.673   |
| This study          | 21.36   |

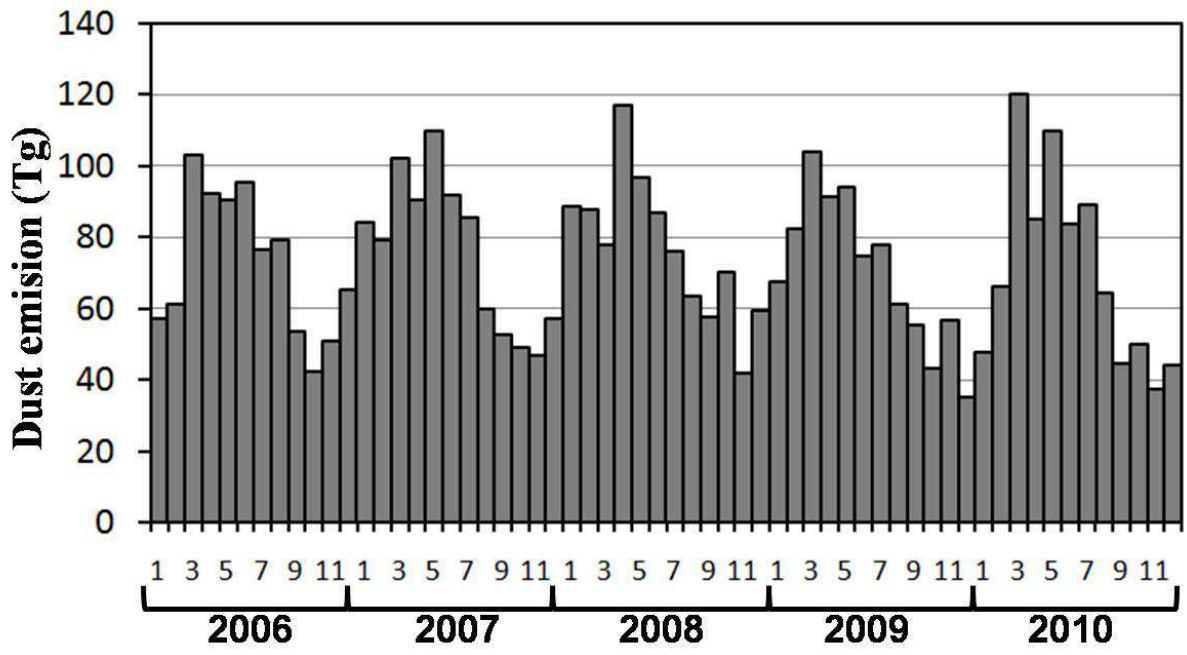
2



1  
2 **Figure 1:** Location of the five AERONET sites used in this study to evaluate the ALADIN  
3 simulated AOT over West Africa Banizoumbou (Niger), Cinzana (Mali), DMN\_Maine\_Soroa  
4 (Niger), MBour (Senegal) and Capo verde.

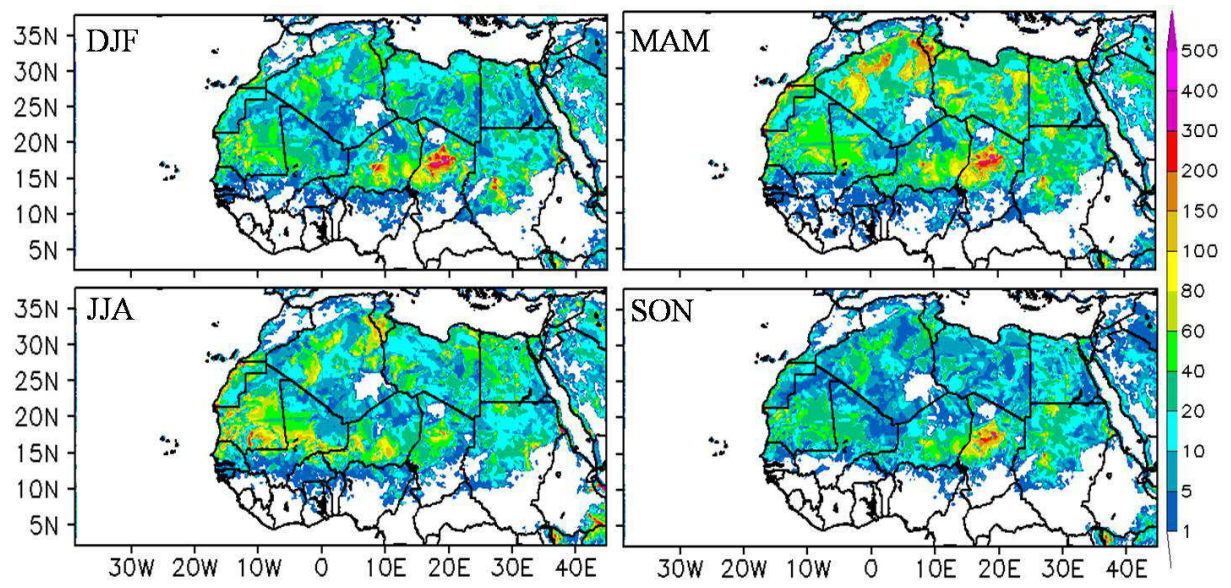


2 **Figure 2:** Annual mean dust emissions (in  $\text{g.m}^{-2}$ ) over North Africa averaged for the 2006-  
3 2010 period simulated by ALADIN.



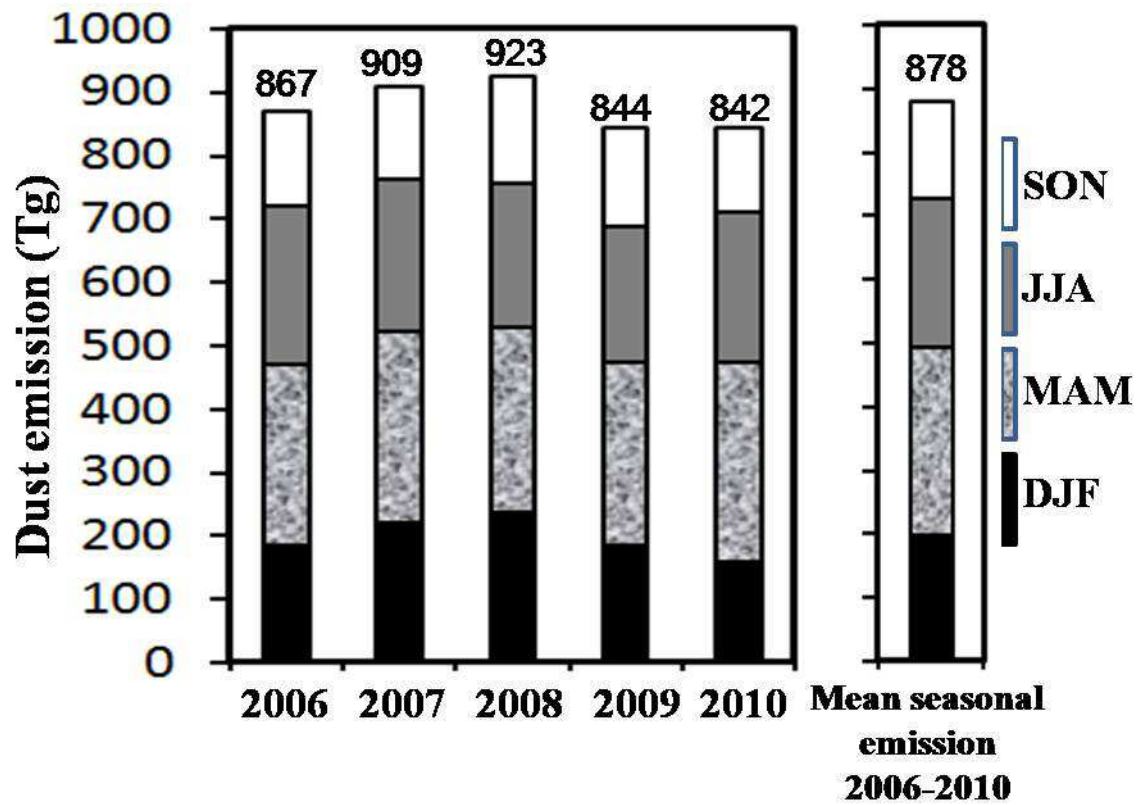
1

2 **Figure 3:** Monthly dust emissions (in Tg) over North Africa from 2006 to 2010 period.



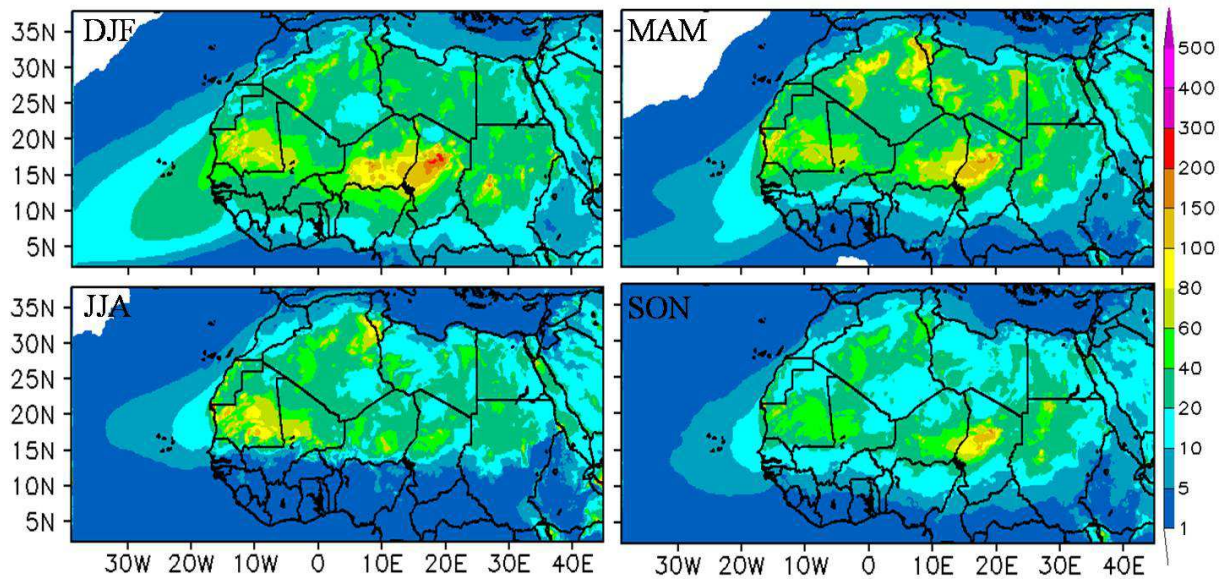
1

2 **Figure 4:** Seasonal mean aerosol dust emissions simulated by ALADIN (in  $\text{g.m}^{-2}$ ) over North  
 3 Africa averaged for the 2006-2010 period.



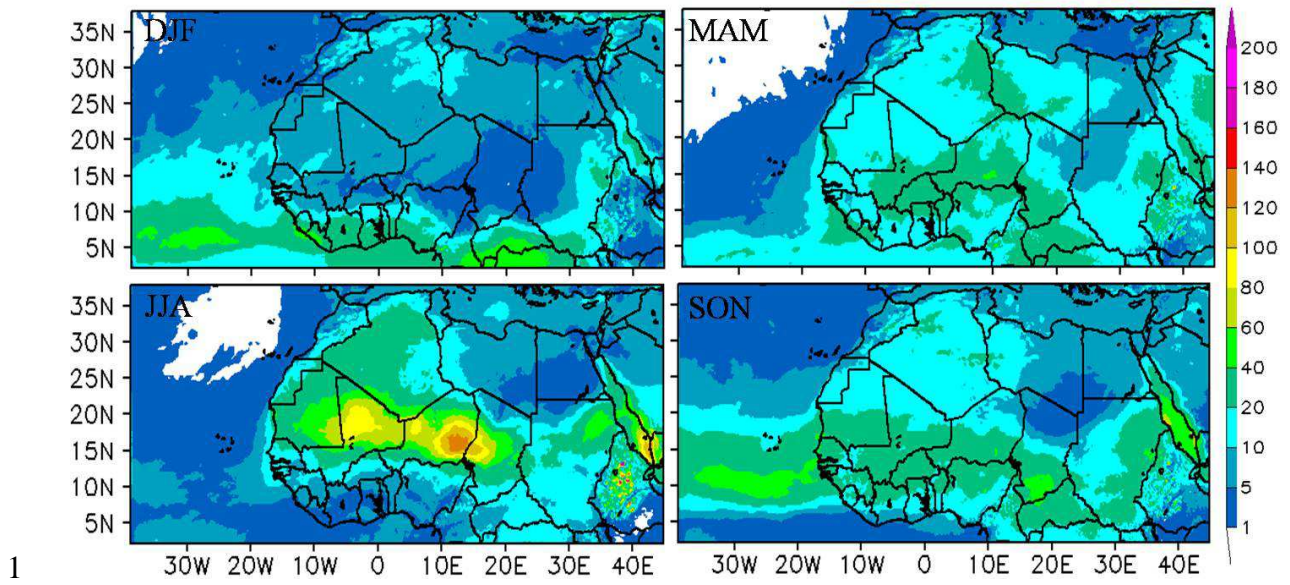
1

2 **Figure 5:** Seasonal mean and interseasonal dust emissions (in Tg) simulated by ALADIN  
 3 over North Africa from 2006 to 2010. The annual average emission is given at the top of each  
 4 bar.



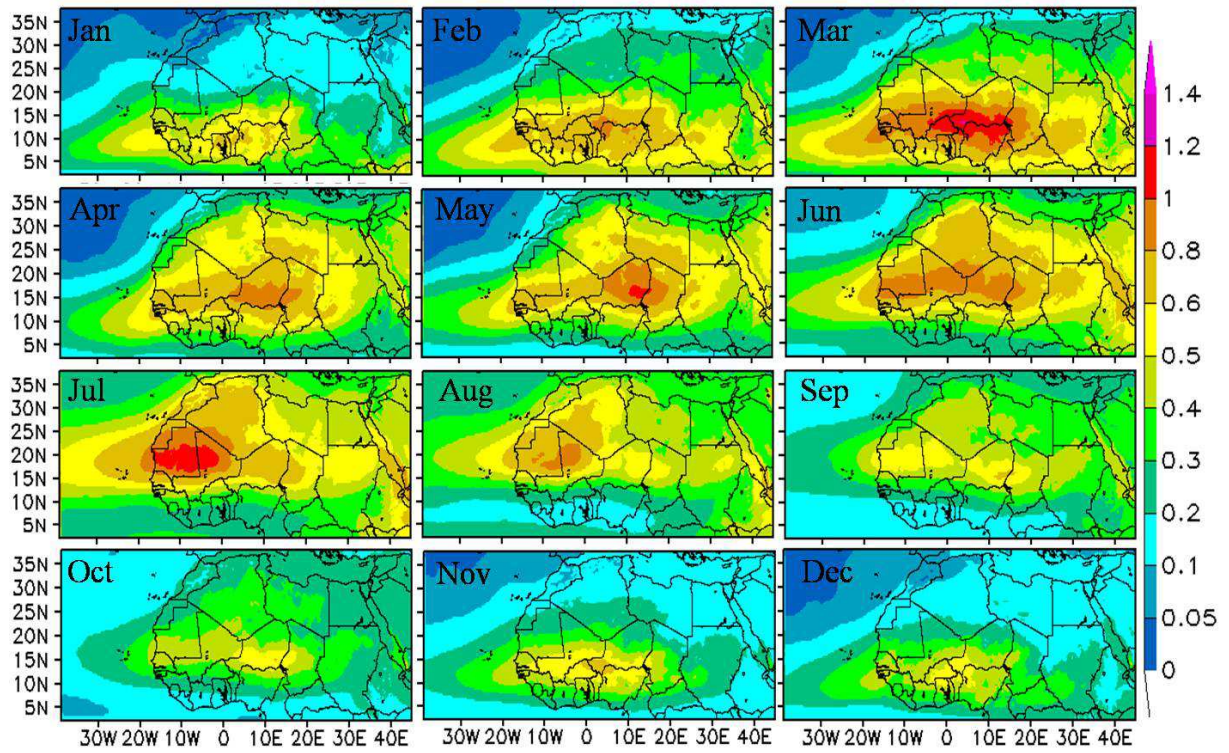
1

2 **Figure 6:** Seasonal mean dry deposition flux simulated by ALADIN (in  $\text{g.m}^{-2}$ ) over North  
 3 Africa averaged for the 2006-2010 period.



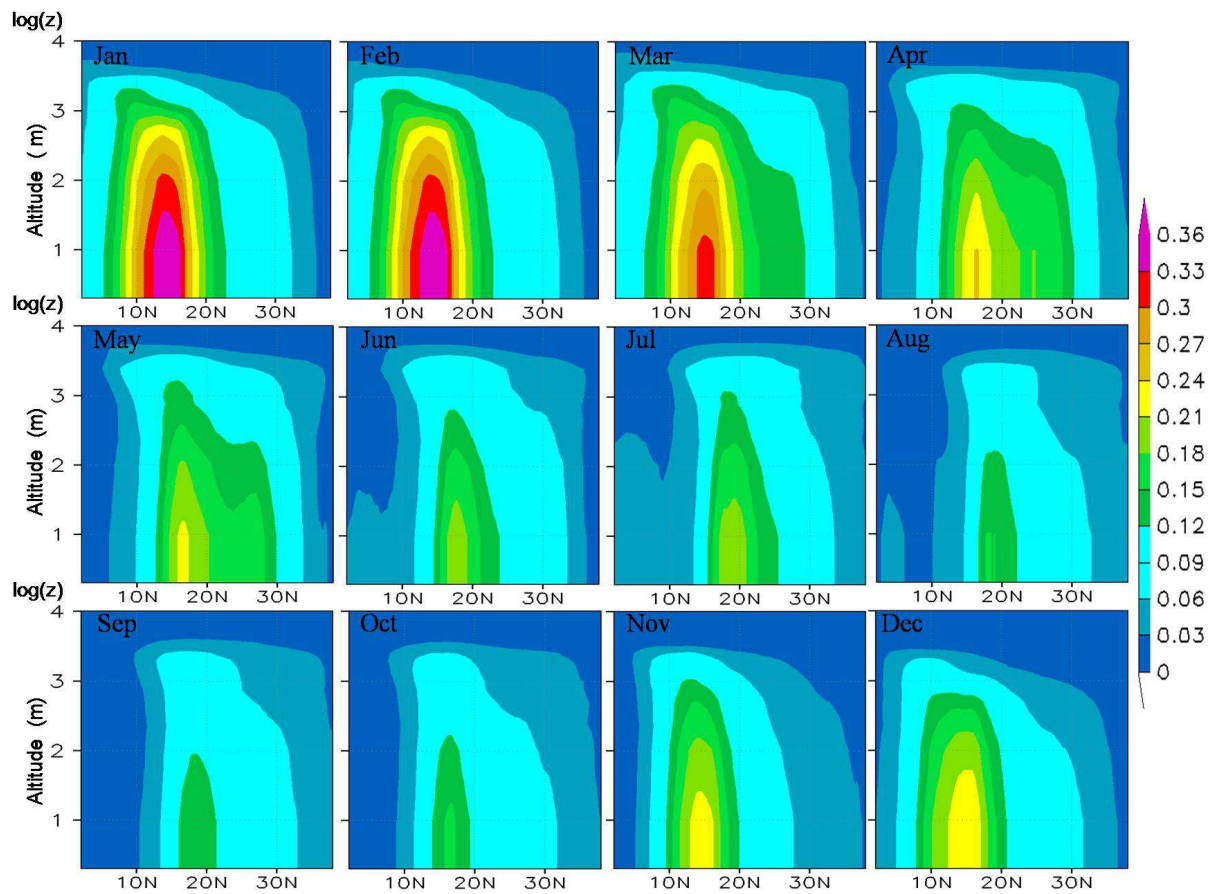
1  
 2 **Figure 7:** Seasonal mean wet deposition flux simulated by ALADIN (in  $\text{g.m}^{-2}$ ) over North  
 3 Africa averaged for the 2006-2010 period.





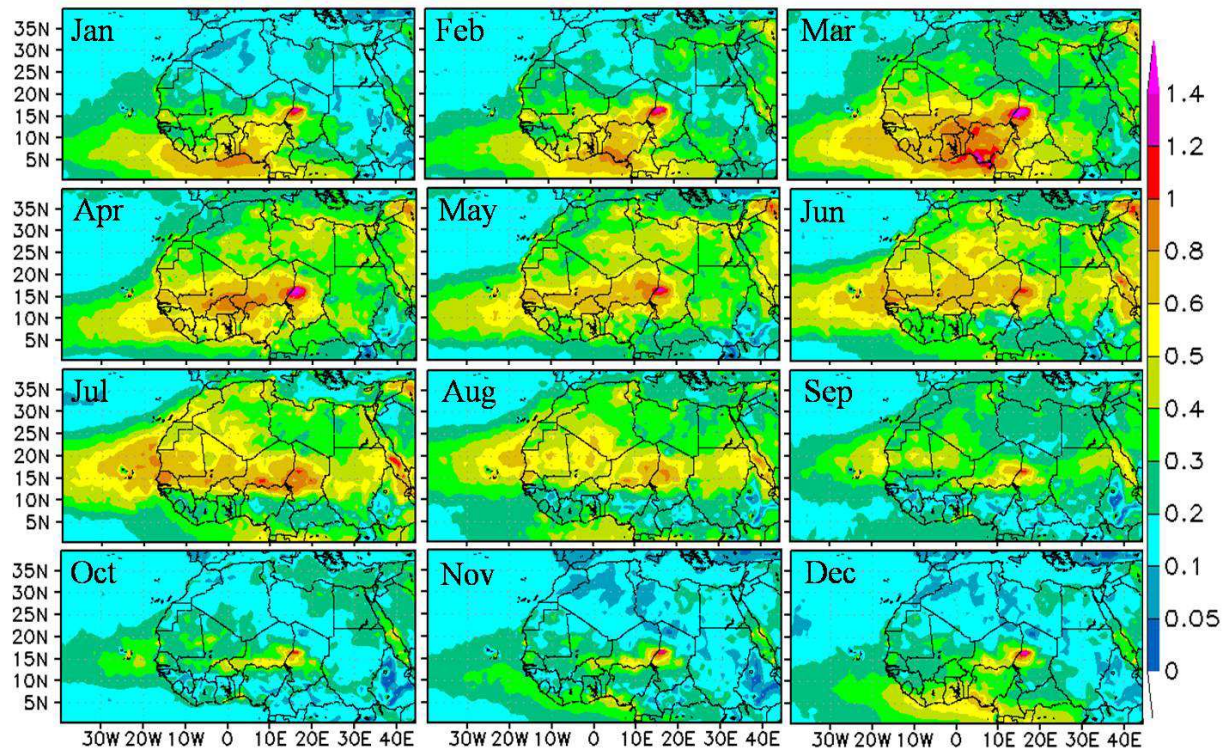
1

2 **Figure 8:** Monthly Aerosol Optical Thickness (AOT) simulated by ALADIN averaged over  
 3 the 2006-2010 period.



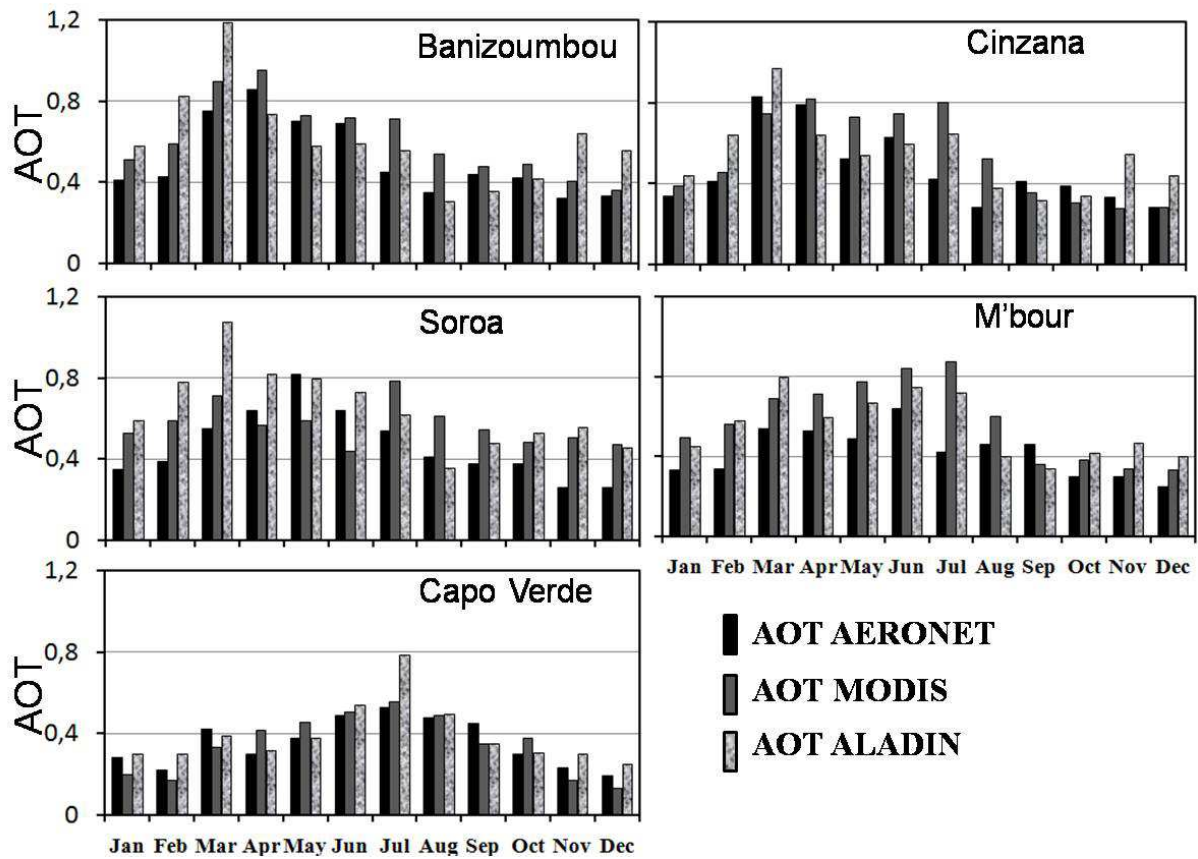
1

2 **Figure 9:** Monthly vertical cross section ( $30^{\circ}$  W -  $40^{\circ}$  E) of extinction coefficients (in  $\text{km}^{-1}$ )  
 3 simulated by ALADIN averaged from 2006 to 2010 over North Africa.

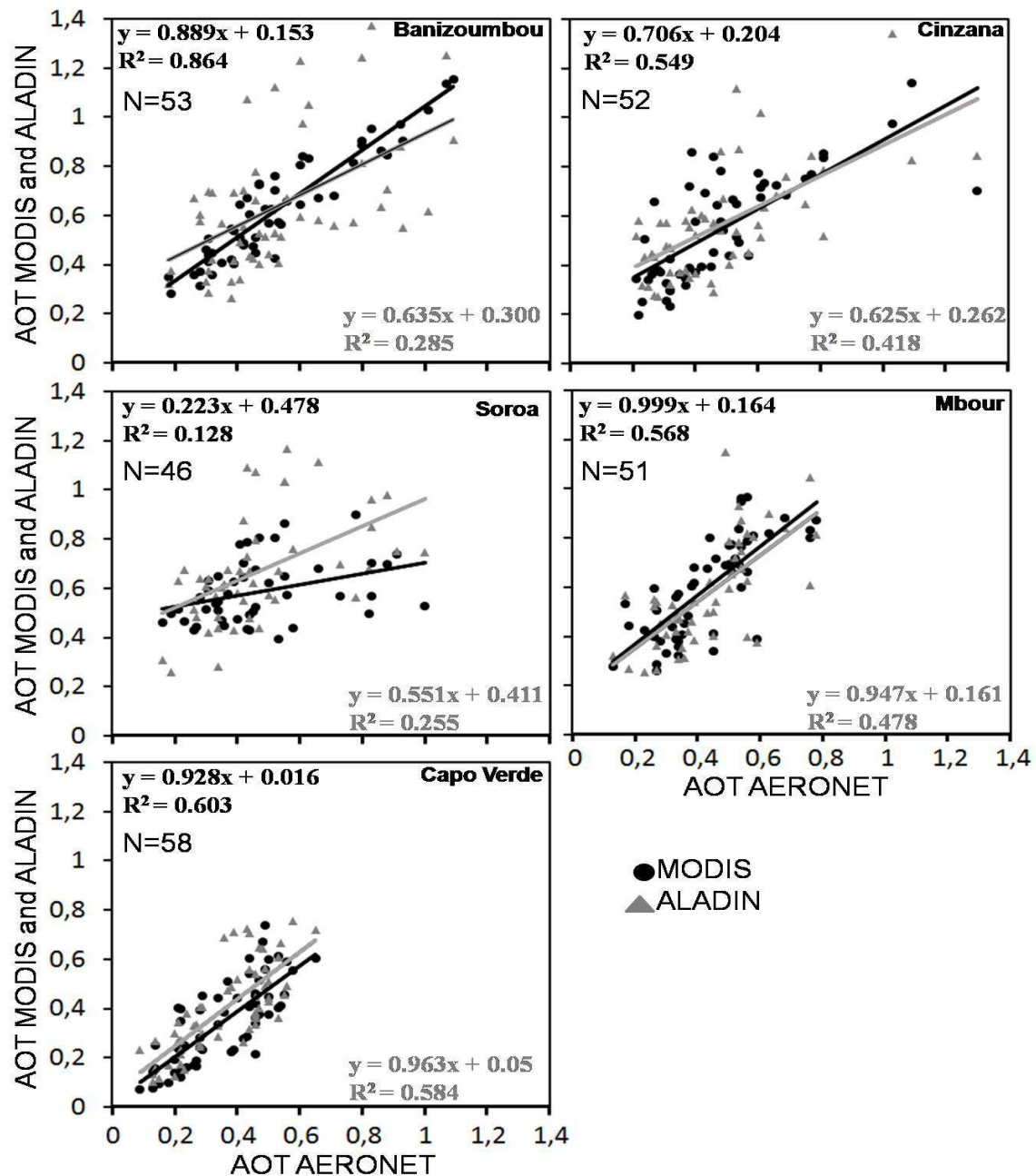


1

2 **Figure 10:** Monthly aerosol optical thickness derived from the combination of the standard  
 3 and Deep Blue products applied to AQUA/MODIS data over North Africa for the 2006-2010  
 4 period.

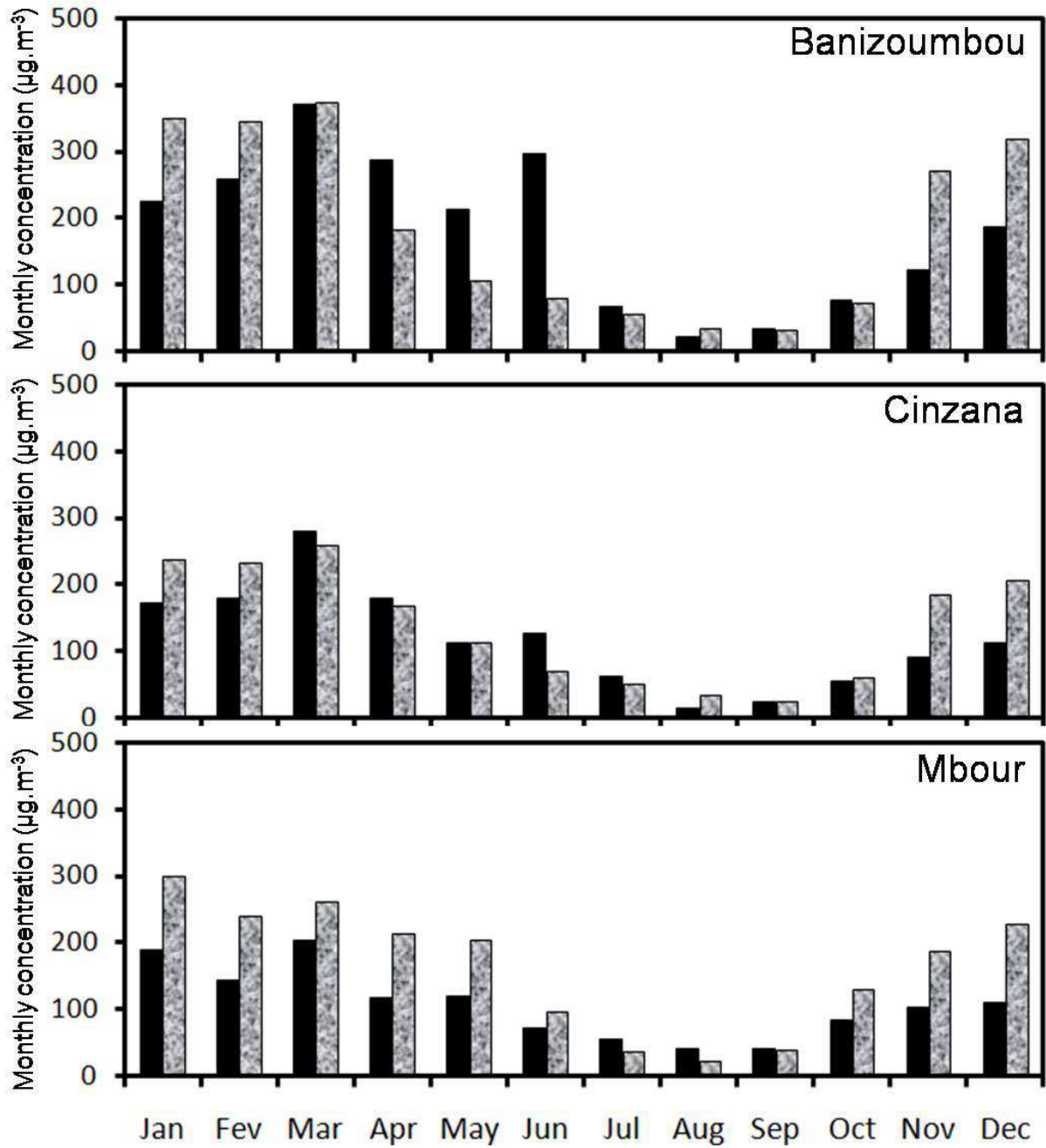


1  
 2 **Figure 11:** Monthly aerosol optical thickness observed by sun photometer (black), MODIS  
 3 (dark gray) and simulated by ALADIN (gray) averaged from 2006 to 2010 over Banizoumbou  
 4 (13°32'2"N, 2°39'54"E), Cinzana (13°16'40"N, 5°56'2"W), Soroa (13°13'1"N, 12°1'22"E),  
 5 Mbour (14°23'38"N, 16°57'32"W) and Capo Verde (16°43'58"N, 22°56'6"W).



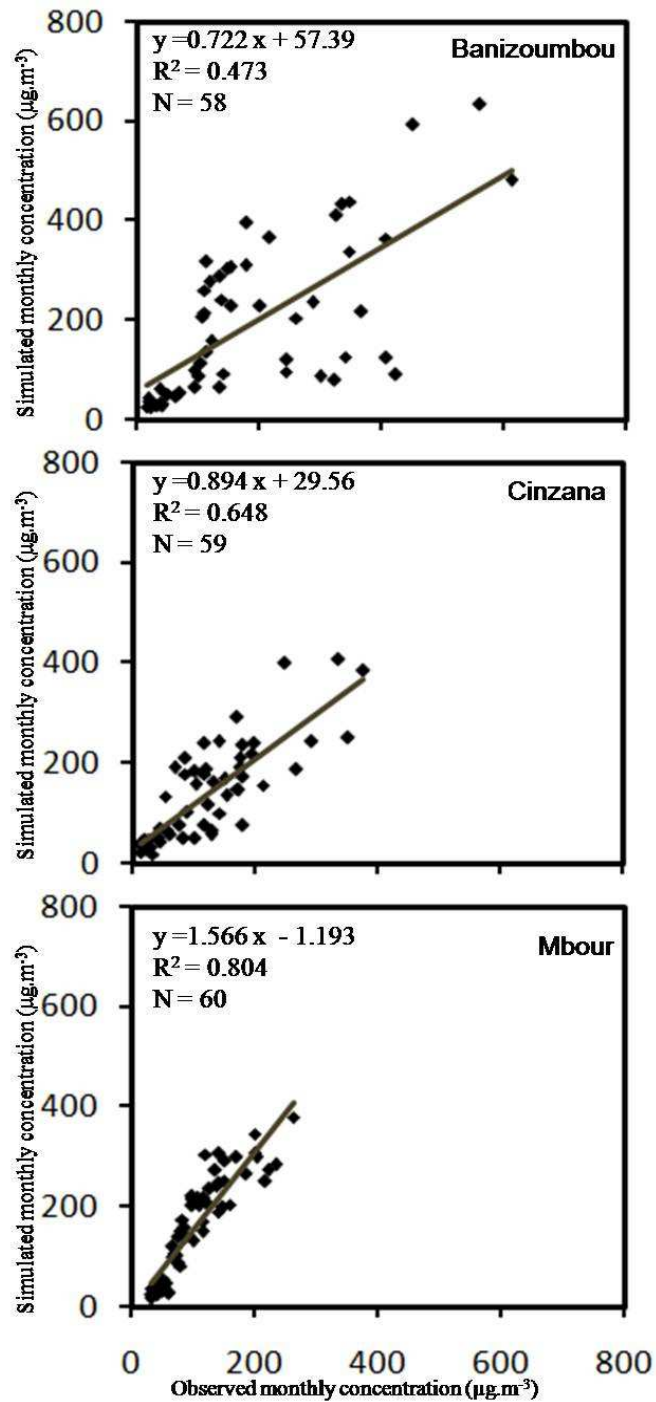
1

2 **Figure 12:** Scatter plot of monthly ALADIN (gray) and MODIS (black) aerosol optical  
 3 thickness against AERONET measurements over Banizoumbou, Cinzana, Soroa, Mbour and  
 4 Capo Verde from 2006 to 2010. In abscissa, AERONET measurements; in ordinate, ALADIN  
 5 and MODIS AOTs. N is the number of averaged monthly data of AOT available from 2006 to  
 6 2010. Each marker represents the averaged monthly AOT from 2006 to 2010. R is the  
 7 correlation coefficient.

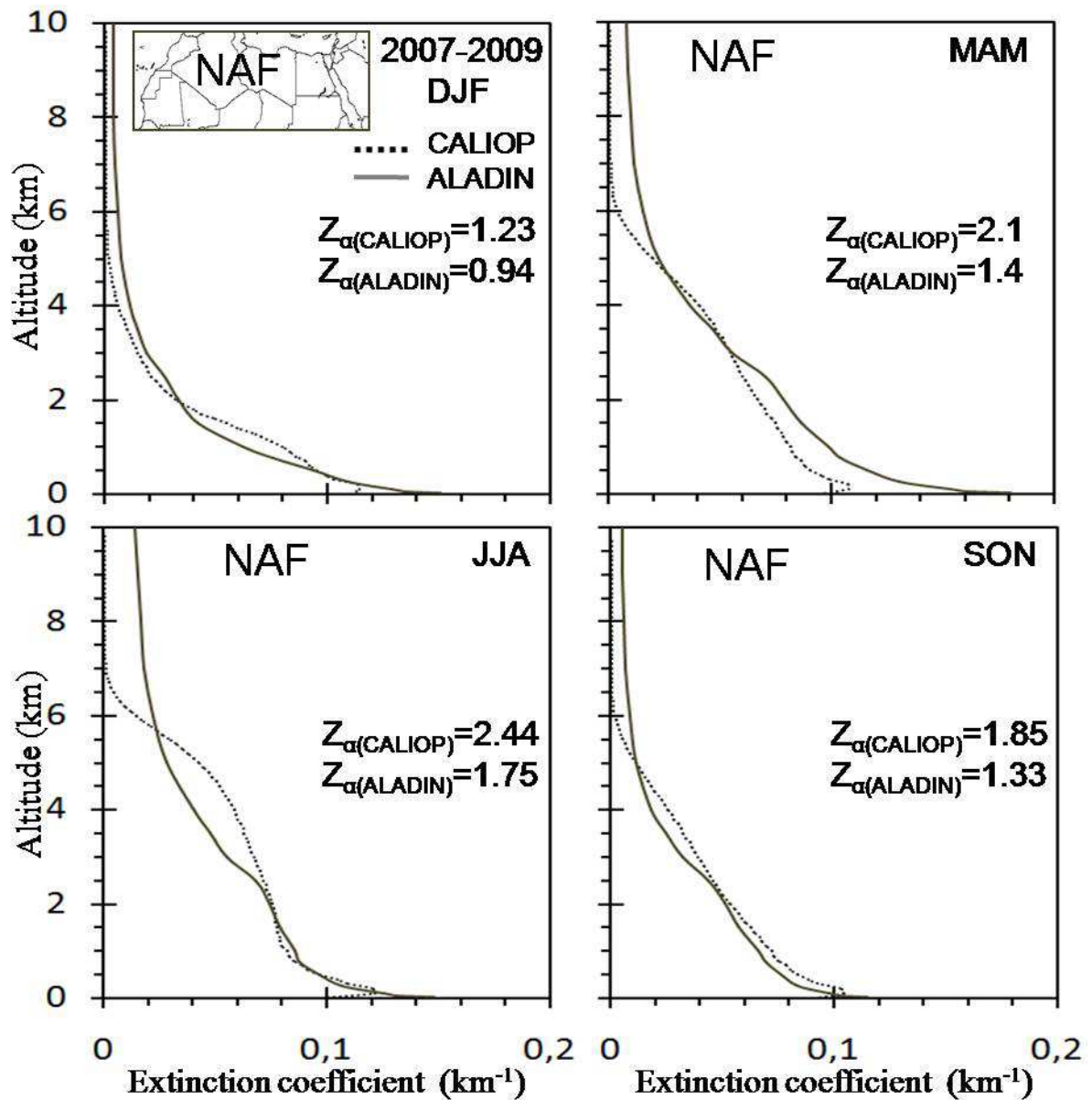


1  
 2 **Figure 13:** Monthly mean of daily median measured (black) and simulated (grey) surface  
 3 concentration (in  $\mu\text{g.m}^{-3}$ ) in Banizoumbou, Cinzana and M'bour from 2006 to 2010.

4



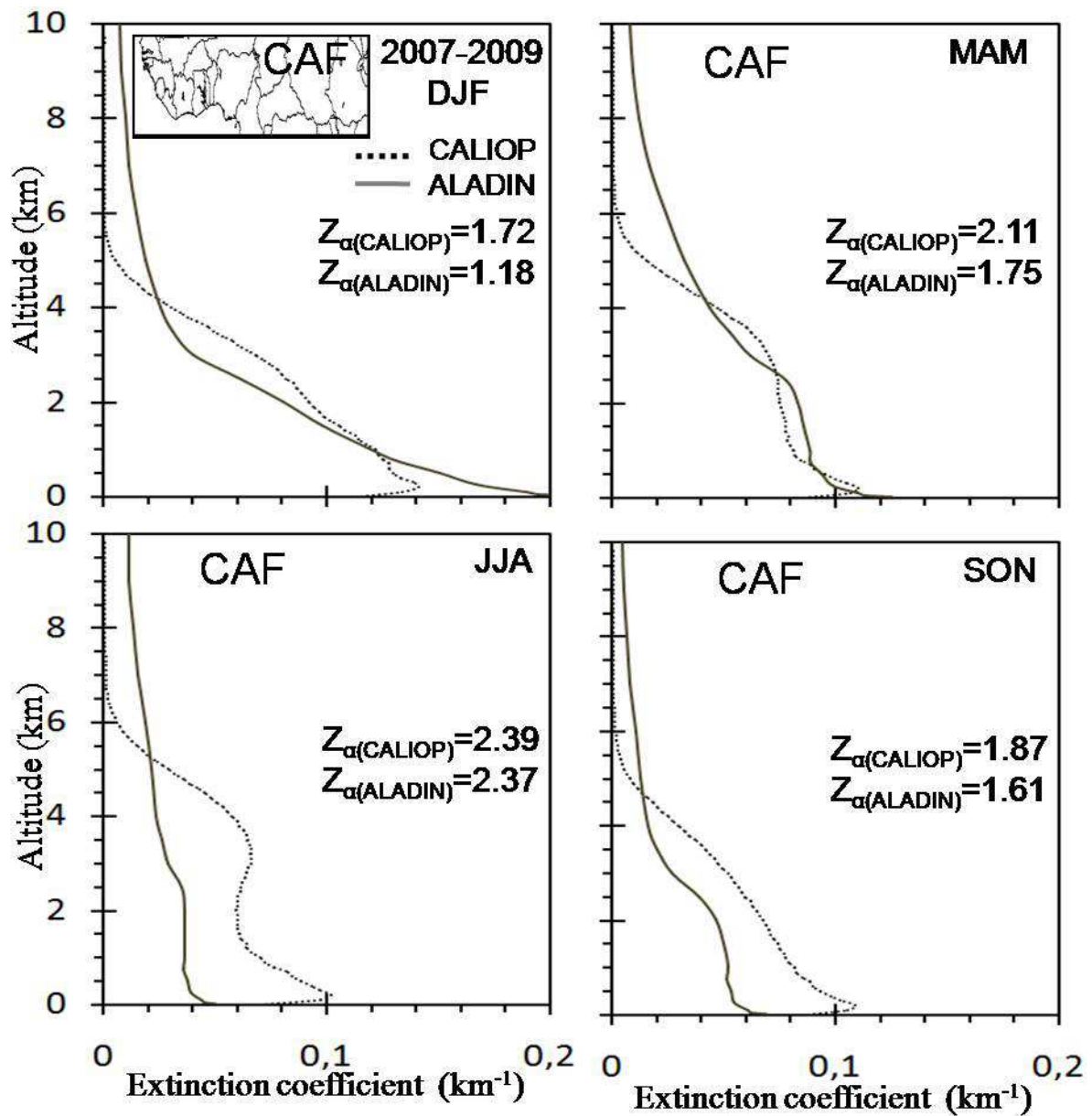
1  
2 **Figure 14:** Scatter plot of monthly ALADIN dust surface concentration against observation  
3 over Banizoumbou, Cinzana and Mbour from 2006 to 2010. N is the number of averaged  
4 monthly surface concentration data available from 2006 to 2010. R is the correlation  
5 coefficient.



1

2 **Figure 15:** CALIOP and ALADIN mean seasonal extinction coefficient (km<sup>-1</sup>) profiles (at  
 3 532 and 550 nm, respectively) averaged from 2007 to 2009 over North Africa (NAF).  
 4 CALIOP profiles are shown as dark dashed lines and ALADIN profiles are shown as  
 5 continuous grey lines. For each season, we give the Z<sub>α</sub> value for CALIOP and ALADIN.





1  
2 **Figure 16:** CALIOP and ALADIN mean seasonal extinction coefficient (Km<sup>-1</sup>) profiles (at  
3 532 and 550 nm, respectively) averaged from 2007 to 2009 over North Africa (CAF).  
4 CALIOP profiles are shown as dark dashed lines and ALADIN profiles are shown as  
5 continuous grey lines. For each season, we give the Z<sub>α</sub> value for CALIOP and ALADIN.